Journal of Renewable and Sustainable Energy REVIEW pubs.aip.org/aip/rse

Methane catalytic cracking by solid materials and molten media for hydrogen production: A review

Cite as: J. Renewable Sustainable Energy **16**, 022701 (2024); doi: 10.1063/5.0188819
Submitted: 24 November 2023 · Accepted: 9 February 2024 ·
Published Online: 1 March 2024

Lei Guo, Jinchi Tan, Junyue Ren, and Zhancheng Guo[a)]

AFFILIATIONS

State Key Laboratory of Advanced Metallurgy, University of Science and Technology Beijing, Beijing 100083, China

[a)]Author to whom correspondence should be addressed: zcguo@ustb.edu.cn

ABSTRACT

Excessive emission of carbon dioxide is the leading cause of global warming. Hydrogen has the advantages of high calorific value and zero carbon emissions. It is considered an ideal energy to solve the problem of global warming, so the demand for hydrogen is increasing yearly. Due to economic considerations, methane is the main raw material for hydrogen production. Currently, 48% of the world's hydrogen comes from steam methane reforming. However, this process needs to burn some methane for heating, generating carbon dioxide emissions simultaneously. In order to avoid carbon emissions from hydrogen production, there is an urgent need to develop new methods to produce hydrogen from methane. Because the carbon generated from direct methane cracking exists in solid form while not as carbon dioxide, the direct methane cracking process for hydrogen production has become a hot research topic in recent years. In this paper, a comprehensive review of the research related to catalytic methane cracking for hydrogen production is presented, especially the research on catalytic cracking of methane using solid materials or molten metal media as catalytic media is summarized in detail. Next, a brief overview of the mechanism of catalytic methane cracking for hydrogen production and the characteristics of the generated carbon as a by-product are presented. Finally, the catalytic cracking of methane in molten media or solid materials and the research trend were prospected.

I. INTRODUCTION

The activities of human societies require the consumption of large amounts of fossil energy, which leads to the emission of large amounts of greenhouse gases, causing global warming. The concentration of carbon dioxide in the atmosphere in 2018 was 410 ppm, an increase in almost 50% compared to 250 years ago.[1,2] Global warming may accelerate the release of methane (whose greenhouse effect is more than 30 times stronger than CO_2) from many natural reservoirs in terrestrial and marine ecosystems, creating a further vicious cycle.[3] If no effective action is taken, more severe environmental and ecological problems such as freshwater depletion, ocean acidification, rising sea levels, and species extinction will gradually emerge. Vigorous development of clean and renewable energy can alleviate the current high dependence on fossil energy for social development. Hydrogen is the richest and simplest element in the universe, and it is a green, clean, and multipurpose energy source or energy carrier. The calorific value of hydrogen combustion is as high as 39.4 kWh kg^{-1}, and only water is produced after combustion.[4,5] Hydrogen energy is known as the "ultimate energy source" for controlling the rise of the earth's temperature and solving the energy crisis in the 21st century because it has the advantages of wide source, high calorific value of combustion, high energy density, zero pollution, and zero carbon emission.[6]

Hydrogen is mainly used in ammonia production, oil refining, and metallurgical industries.[7–9] Also, because the hydroxide fuel cell can directly convert chemical energy into electrical energy, breaking through the limit of Carnot cycle efficiency, it also has a broad application in automobile power and power generation.[10,11] With the development of the economy, the demand for hydrogen in the industrial field has been increasing yearly. The increase in the demand for hydrogen is more than three times in 2018 compared with 1975.[12] With the rapid development of solid hydrogen storage materials,[13–16] in the future, hydrogen energy will also enter the fields of transportation, power generation, and buildings by blending it into the natural gas network in homes and commercial buildings, where it can be used for combustion for heating; in addition, the use of hydrogen in gas turbines can increase the flexibility of the power system. In summary, the demand for pure hydrogen will increase significantly in society in the future, which challenges existing hydrogen production processes,

so new efficient and low carbon emission hydrogen production processes need to be developed.

Currently, 96% of the world's hydrogen is prepared from fossil energy as a primary feedstock. Due to the advantages of low production cost and relative maturity of the process, steam methane reforming (SMR) to hydrogen accounts for 48% of the total hydrogen production.[17] However, the process also has shortcomings, such as high energy consumption (1/3 of the methane input is directly used for combustion for heat) and high carbon emissions (9–12 kg CO_2/kg H_2),[18] which makes it contrary to the current stringent environmental policies and the low-carbon economy. Some hydrogen production technologies are based on renewable energy sources, such as water electrolysis (accounting for 4% of global hydrogen production)[19,20] and methane pyrolysis by solar power,[21,22] etc. However, renewable-energy-based hydrogen production technologies are still not yet applied on a large scale for practical production because of cost and technical reasons. Figure 1 illustrates the methods of traditional hydrogen production and the applications of hydrogen.

As the cost of extracting natural gas from unconventional reservoirs such as shale gas decreases, methane resources will become abundant and affordable in the coming decades.[23] So, using methane as a feedstock for hydrogen production is still a trend in the future. Although the current SMR process for hydrogen production is mature, its hydrogen production process still emits excessive CO_2.[24] In order to solve the carbon emission problem of SMR hydrogen production, the CO_2 produced needs to be captured and sequestered, which makes the SMR technology face many challenges, so there is a great need to find better alternatives for methane hydrogen production.

In the last two decades, many scholars have begun to study new methods of hydrogen production, mainly methane cracking, the method of heating methane so that it is directly cracked at high temperature into hydrogen and by-product carbon ($CH_4 \rightarrow 2H_2 + C$); the most significant feature is that it does not produce CO_2 gas, the by-product carbon is more accessible to collect and store compared to CO_2 if the solid carbon is purified, processed, and handled, and it is expected to be turned into high value-added graphene or nanocarbon materials. However, methane is a regular tetrahedral structure. High energy must be absorbed to break the high-energy C–H bonds, so methane's noncatalytic cracking must occur at high temperatures (≥1200 °C).[25] To solve the disadvantage that methane pyrolysis requires high-temperature conditions, researchers have reduced the activation energy of methane cracking by adding catalysts, reducing the cracking temperature and the supply heat of the cracking process. For example, solid catalysts such as activated carbon,[26] carbon black,[27,28] metallic materials,[29–32] and natural iron ore[33] were used for catalytic cracking of methane. With the addition of solid catalysts, methane can be cracked between 600 and 900 °C, the cracking temperature is significantly decreased, and a good methane conversion can be achieved. However, the solid catalyst-catalyzed methane cracking has a new problem, i.e., the solid carbon generated during the cracking process will be deposited on the solid catalyst's surface, resulting in the solid catalyst's poisoning, coking, and deactivation.[34,35] The regeneration process of the deactivated catalyst requires oxidation of the carbon covered on the catalyst surface, generating additional CO_2 emissions.[36,37] To solve this problem, a new process using molten metal-catalyzed methane cracking for hydrogen production has emerged in recent years to solve the problem of not making continuous methane cracking due to catalyst deactivation.

Many scholars have summarized the research on hydrogen production from methane pyrolysis. Fan[7] introduced the development history of hydrogen production from methane cracking, the mechanism of cracking, and the study of catalytic systems, focusing on how to solve the problem of catalyst deactivation. Figure 2 shows the development history of the hydrogen production process by catalytic cracking of methane. Kannah[38] analyzed the economic sensitivity of different hydrogen production processes and summarized the advantages and disadvantages of each process. In addition, several papers have also summarized the preparation, catalytic effect, reactivity, reaction stability, and regeneration of metal-based catalysts in more detail.[37,39,40] McConnachie[41] summarized the cracking effect of

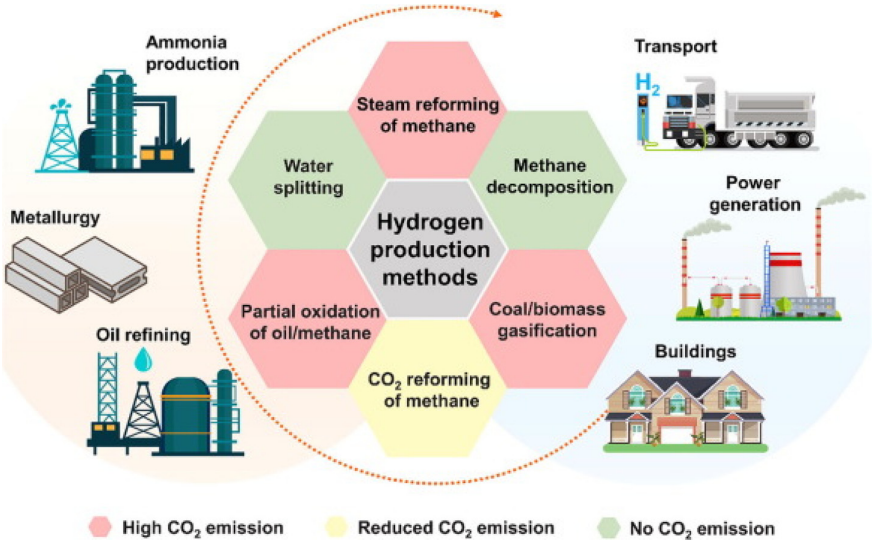

FIG. 1. Conventional hydrogen production methods and hydrogen applications.[7] Reproduced with permission from Fan *et al.*, J. Energy Chem. **58**, 415–430 (2021). Copyright 2021 Elsevier BV.

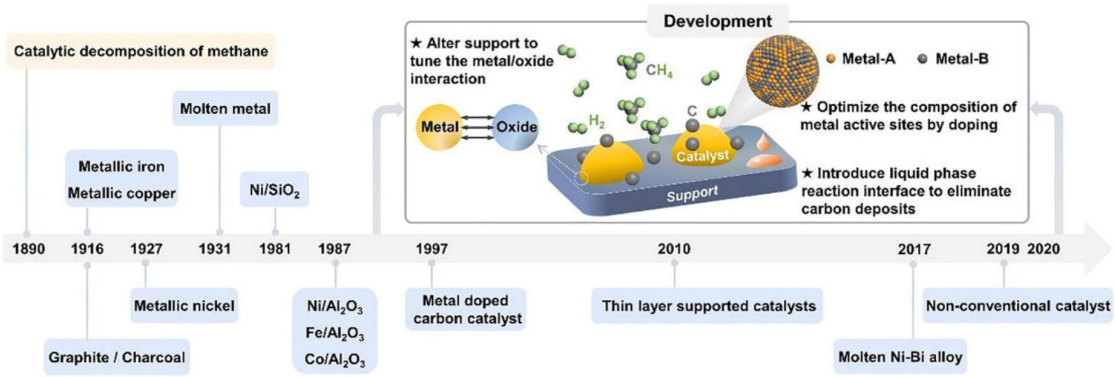

FIG. 2. Research history of catalytic cracking of methane.[7] Reproduced with permission from Fan *et al.*, J. Energy Chem. **58**, 415–430 (2021). Copyright 2021 Elsevier BV.

methane in different reactors and the mechanism of the by-product carbon generation, aiming to advance the design of methane cracking reactors and the process of methane cracking for hydrogen production toward commercialization. Msheik[42] comprehensively reported the development studies of molten media as catalytic media for hydrogen production from methane cracking and using solar heat cracking reactors. It concluded that the hydrogen production method with a novel molten media solar reactor would be a promising pathway for clean hydrogen production.

Experimental research on hydrogen production from the catalytic cracking of methane has continued for decades. However, there is still no report on applying the methane cracking process for hydrogen production in actual production. No suitable catalytic medium and cracking process have been found in the final analysis. This paper summarizes the methods and effects of different catalysts in catalytic methane cracking to produce hydrogen, aiming to provide a reference for selecting catalytic media and the corresponding cracking process for methane catalytic cracking. First, starting from the research history of methane cracking, this paper provides an overview of the catalytic effect of solid catalysts (metal-based and carbon-based) on methane cracking, emphasizing and summarizing the research on methane cracking with inexpensive iron-based catalytic materials. Then, the experimental research on the clean and low-carbon molten media (including mono-metallic, alloys, and molten salts) catalyzed methane cracking to produce hydrogen is described in detail. Finally, the mechanism of methane cracking and the morphology characteristics of carbon as a by-product are outlined at the same time. Moreover, the research direction of the molten metal methane cracking process and the solid catalysts used for catalyzing methane cracking are outlooked. These are expected to provide some references for the scholars in this field.

II. SOLID CATALYSTS

Although there is no CO_2 gas emission from the methane cracking process, the direct cracking of methane needs to be carried out at higher than 1200 °C. Scholars have reduced the temperature of the methane cracking process by adding solid catalytic media (mainly carbon, nickel, and iron) to reduce the energy consumed by the methane cracking process and increase the cracking rate simultaneously.

A. Carbon-based catalysts

The use of carbon-based catalysts for methane cracking has been explored due to the excellent adsorption capabilities of activated carbon. Pinilla *et al.*[43] blew pure methane at a 20 ml (STP)/min flow rate into a quartz fixed-bed reactor containing an industrial activated carbon (CG Norit). 60% conversion of methane could be achieved at 850 °C, and the reaction life of the activated carbon was more than 8 h. In the deactivation–regeneration cycle experiment of the catalyst, it was found that the surface area and the oxygen-containing groups on the surface of the deactivated catalyst after activation by CO_2 were linearly and positively correlated with the degree of combustion (the ratio of the mass of the deactivated catalyst that had been gasified during the regeneration process to its mass prior to regeneration), which means that the more the deactivated catalyst was gasified during the regeneration process, the more the surface area would be more significant after regeneration. In addition, since the gasification resistance of the activated carbon regeneration process decreases, the researchers believe that the activated carbon removes its residual portion in each regeneration process. After three regeneration treatments, the activated carbon is wholly gasified. The final carbon obtained is the deposited carbon generated by methane cracking.

Harun *et al.*[44] blew 50 vol. % N_2 and 50 vol. % CH_4 into a nickel–chromium–iron alloy fixed bed containing biologically activated carbon (referred to as AB) at a temperature of 800 °C to obtain 69% methane conversion. In contrast, 73% methane conversion was achieved over an industrial activated carbon catalyst (Ru-AC) containing 3 wt. % Ru. After 60 h of reaction, Ru-AC was deactivated. At that time, the methane conversion was only 21%, but on AB, the methane conversion still reached 51% due to the high specific surface area of AB (3250 m^2/g); meanwhile, AB contains alkali metals, which led to carbon nanotubes (CNTs) being generated by methane cracking, and the formation of the carbon nanotubes significantly extended the reaction lifetime of AB.

Wang *et al.*[45] made an iron-doped carbon catalyst by adding iron nitrate to Shenmu sub-bituminous coal, which KOH subsequently activated. A 20 vol. % CH_4 and 80 vol. % N_2 mixture was blown into the reactor at 850 °C and atmospheric pressure. The experimental results showed that with the increase in the Fe content, the methane conversion increased significantly, although the surface area of the

catalyst decreased. The highest catalyst activity was observed when the Fe content reached 30 wt. %. The conversion of CH_4 increased from the initial 20% to 58% after the reaction was carried out for 9 h. The reason was that the carbon catalyst was deposited by the carbon generated from methane cracking on the pores at the early stage of the reaction and then rapidly deactivated, and the deactivated carbon became a support of Fe. At the late stage of the methane cracking reaction, Fe played a catalytic role, so the conversion increased significantly. In addition, the carbon produced by methane cracking reduced the size of Fe particles, which led to improved Fe dispersion, so the catalyst activity was enhanced with time. The Fe-doped carbon-based catalysts obtained at carbonization temperatures of 800 and 850 °C exhibited relatively high activity and stability, and the total specific surface area and pore volume of the catalysts decreased with increasing carbonization temperature.

Zhang *et al.*[46] used coal liquefaction residue as a precursor, then activated it with KOH, added some Al_2O_3, and finally prepared a hierarchical micro-/macro- mesoporous AlRC catalyst. These catalysts showed excellent catalytic effects, increasing methane conversion from 27% to 61% after 10 h. The result is mainly caused by the accumulated active fibrous carbons because when the produced fibrous carbons serve as the catalyst for methane cracking, new fibrous carbons can be formed. Hence, the conspicuous activity of the fibrous carbon gradually increases the methane conversion on AlRC.

Many scholars have conducted experiments on the catalytic cracking of methane using carbon black and activated carbon and have compared the catalytic performance of the two types of catalysts. Several studies have reached similar conclusions: the carbon black still exhibits stable activity after a short reaction period, and the activation energy for the catalytic cracking of methane on commercial carbon black is lower than that on activated carbon. Despite significant changes in the surface area and morphology of the carbon black during the cracking reaction, the activity remained unchanged until the crystalline carbon produced by methane cracking coated the surface of the carbon black on a large scale, and the carbon black lost its activity. In addition, the surface chemistry of the carbon and the distribution of the pore sizes have essential effects on the initial methane conversion and the catalyst's long-term stability.[27,28,47–49]

B. Nickel-based catalysts

Nickel has good catalytic properties for methane cracking, and in recent years, there have been many reports on nickel-based materials as catalysts for methane cracking. In the study of catalytic cracking of methane using nonsupport nickel-based materials, Pudukudy *et al.*[50] prepared two types of nonsupport porous catalysts (NiO and Fe_2O_3) using a precipitation method. Both types of catalysts were obtained as catalytically active metals Ni and Fe after continuous reduction in a stainless steel tube with an inner diameter of 250 mm and a height of 600 mm with a hydrogen flow of 150 ml/min for 90 min at 600 °C. Pure methane was blown into the reactor at a 150 ml/min flow rate. Maximum hydrogen yields of 66% and 53% were obtained for Ni-based and Fe-based catalysts, respectively, when methane was cracked at 800 °C. Figure 3 demonstrates the carbon morphology of the by-products on both types of catalysts, with metal-coated carbon nano-blocks on Ni-based catalysts and multilayered graphite flakes on Fe-based catalysts. Both types of catalysts were not deactivated after 6 h of reaction. Because the diffusion rate of carbon in Fe is higher than that of Ni, the Fe-based catalysts have higher catalytic stability.

Zhou *et al.*[51] prepared an unsupported ME-$Ni_{88}Pt_{12}$ alloy catalyst by (ME stands for microemulsion) the water-in-oil (W/O) microemulsion method. This catalyst presents a stable methane conversion (about 55%) at 700 °C for 1 h at a F/W = 12 l/(gcat h). The author thought the reason may be that the formed Ni–Pt alloy tunes the carbon deposition, diffusion, and graphite formation rate to a balanced state, which favors the CNT growing and then anchoring the metal on the tip of the CNT. The Ni–Pt alloy on the tip of CNT thus maintains the stable methane cracking activity.

Because the support in the catalyst significantly reduces the amount of catalytic metal used, most subsequent studies have used nickel-based catalysts containing oxide supports.

Venugopal *et al.*[52] investigated the effect of Ni content in Ni/SiO_2 catalysts on methane cracking. The result showed that among all catalysts, 30 wt. % Ni/SiO_2 has a better performance at 600 °C. When the loading amounts exceed 30 wt. %, the catalytic performance decreases rapidly. This is because the catalytic performance of Ni/SiO_2 depends on the amount of Ni and the size of the nickel particles. When the Ni exceeded 30 wt. %, the size of Ni metal particles increased sharply (21–40 nm) because the accumulation of nickel particles occurred during the reduction of catalyst, so 30 wt. % Ni/SiO_2 has suitable Ni content and nickel particles size (about 21 nm), and it has a better performance.

Through experiments, Takenaka *et al.*[53] found that among all M–Ni/SiO_2 catalysts (M stands for Cu, Rh, Pd, It, and Pt), Pd–Ni/SiO_2 has the best effect and longer life in catalytic cracking methane, and then investigated the performance of the Pd–Ni catalysts loaded on different supports, the supports are CF (carbon fiber), MgO, Al_2O_3, SiO_2, and TiO_2. The results showed that Pd–Ni/MgO showed a low activity for the methane decomposition, while the catalytic activities of Pd–Ni/TiO_2, Pd–Ni/SiO_2, Pd–Ni/Al_2O_3, and Pd–Ni/CF were high. This is because Pd–Ni/MgO Ni species in the catalyst form the $NiMgO_x$ solid solutions and were not reduced easily into active Ni metal, while Ni species in Pd–Ni/TiO_2, Pd–Ni/SiO_2, Pd–Ni/Al_2O_3, and Pd–Ni/CF were present as Ni metal mainly. Second, they founded that branched carbon nanofibers (CNFs) were formed in Pd–Ni/CF, which improved the performance and lifetime of the catalyst, so Pd–Ni/CF was the best catalyst in their work.

Villacampa *et al.*[54] prepared 30 wt. % Ni/Al_2O_3 methane cracking catalysts by the co-precipitation method. They found that the increase in H_2 concentration decreases the content of carbon deposited on the catalyst, and at the same time, it will prolong the induction period of carbon nucleation, and so reduces the rate of deactivation of the catalyst. However, the increase in CH_4 concentration speeds up the rate of carbon filament generation and the catalyst deactivation rate. Therefore, the competitive effect of H_2 and CH_4 at the Ni surface sites inhibited the generation of carbon filaments and encapsulated pyrocarbon, and therefore prolonged the reaction life of the catalyst.

Amin *et al.*[55] studied the catalytic performance of porous Ni/Al_2O_3 and non-porous Ni/Al_2O_3 catalysts after regeneration. The results showed that the non-porous catalyst showed a rapid decrease in activity after the first cycle and continued to decline in subsequent cycles; after the sixth cycle, it had almost no activity; however, the porous catalyst showed good stability over 24 cycles. There are several reasons for this. First, the non-porous catalyst's regeneration process produces inactive $NiAl_2O_4$, so the total surface area of active nickel

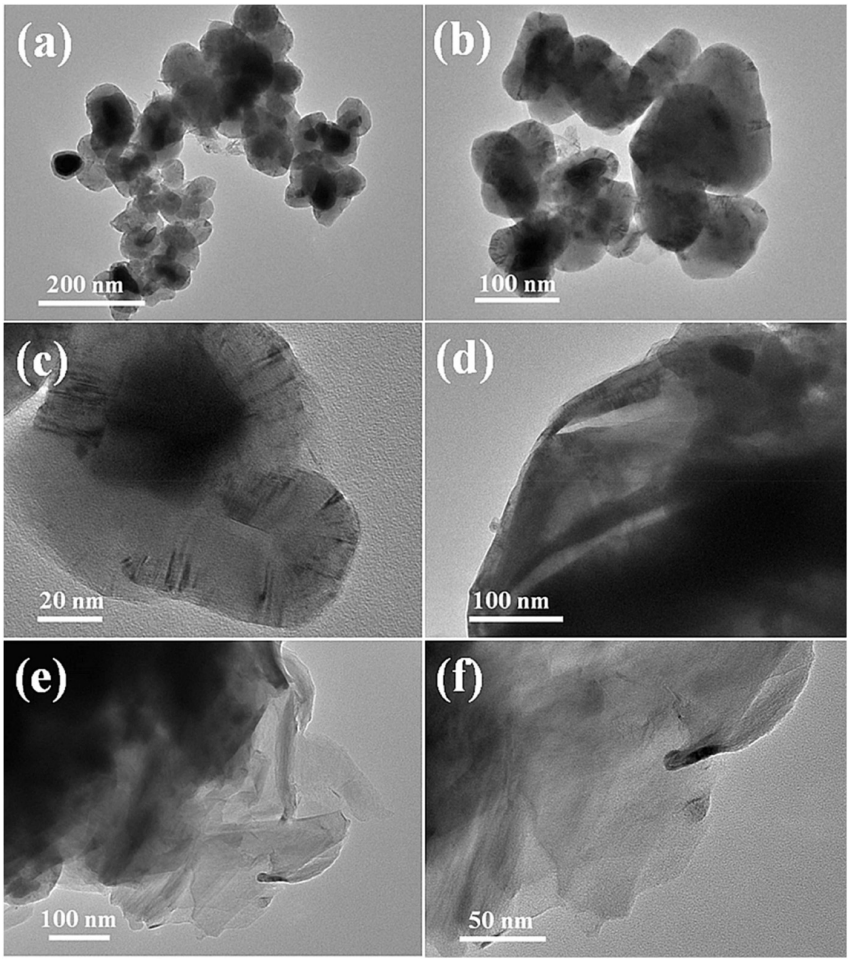

FIG. 3. TEM images of nano-carbons deposited on Ni-based (a)–(c) and Fe-based (d)–(f) catalytic materials.[50] Reproduced with permission from Pudukudy *et al.*, Int. J. Hydrogen Energy **41**, 18509–18521 (2016). Copyright 2016 Elsevier Ltd.

available was reduced. Second, the nickel deposited on the surface of the non-porous catalyst is sintered to form larger clusters, which reduces the dispersion of nickel and prevents the formation of carbon filaments, thus causing the formation of larger carbon agglomerates. Third, Ni is more dispersed on the porous catalyst and less prone to form large Ni clusters. Thus, carbon filaments can grow, which reduces the possibility of sintering and the interaction between nickel and Al_2O_3 support. Therefore, $NiAl_2O_4$ rarely exists in porous catalysts.

Bayat *et al.*[56] used the sol-gel method to prepare γ-Al_2O_3 support and also used the wet impregnation method to prepare 50 wt. % Ni–15 wt. % Pd/Al_2O_3 catalysts, 30 vol. % N_2 +70 vol. % CH_4 was blew into the quartz fixed bed containing catalyst. The highest conversion of methane reached 95% at the beginning of the reaction, and then gradually decreased to 68% after 6 h. The carbon generated from methane cracking was a nanofiber structure. In addition, adding palladium to the nickel-based catalyst improved the reduction performance of the nickel-based catalyst, which increased the catalytic activity. In addition, the formed Ni–Pd alloy improved the methane dissociation performance because the diffusion rate of carbon in palladium is much faster than that in nickel, so the addition of palladium to the nickel-based catalyst inhibited the generation of encapsulated carbon, which led to the extension of the catalyst life. In the study of Ni–Fe/Al_2O_3 catalysts,[57] they found that the introduction of Fe had a similar effect with Pd; that is, the addition of iron to nickel catalyst improved the catalytic stability by enhancing the rate of carbon diffusion and preventing the formation of encapsulating carbon. However, the iron reduced the reducibility of nickel in the catalyst, thus reducing the amount of active metal available. Therefore, adding 10 wt. % Fe to the Ni/Al_2O_3 catalyst is more appropriate.

In addition, regarding the study of nickel-based ternary alloy-loaded catalysts, Bayat *et al.*[58] prepared Al_2O_3 supports by the sol-gel method, and loaded ternary nickel-based catalysts were produced by loading Ni–Fe–Cu based materials onto Al_2O_3 by the impregnation method. It was found that the addition of iron-based materials could enhance the catalytic effect of nickel-based catalysts on methane cracking because iron could increase the diffusion rate of carbon by-products and reduce the amount of encapsulated carbon generated on the surface of Ni, thus improving the stability of the catalysts. However, adding Fe-containing materials inhibited the reduction of Ni-based materials, and the lack of some catalytically active metal Ni

would have some negative effects on methane cracking. In addition, the addition of copper-based materials not only improves the adsorption capacity of methane on the catalyst but also reduces the amount of encapsulated carbon generated on the Ni surface and improves the reducibility of the nickel-based materials and the dispersion of Ni obtained from the reduction on the catalyst surface, which improves the catalytic effect of the catalysts.

In terms of composite supports, Ahmed *et al.*[59] prepared supports CeO_2–Al_2O_3 for Ni-based catalysts by the co-precipitation method and subsequently loaded Ni from $Ni(NO_3)\cdot 6H_2O$ onto CeO_2–Al_2O_3 supports using the impregnation method, and thus, Ni/CeO_2–Al_2O_3 catalysts with different metal-atom ratios were prepared. The Ni/CeO_2–Al_2O_3 catalysts were denoted as Ni/Ce_x–Al_{1-x}. Their experiments showed that the highest hydrogen production rate could be achieved on the Ni/Ce_{25}–Al_{75} catalyst, and it had a relatively high stability. In addition, different kinds of carbon nanostructured materials can be obtained on the catalyst surface due to different CeO_2 contents. Carbon nanofibers (CNFs) appeared on all catalysts containing Al_2O_3. In contrast, only highly graphitized multi-walled carbon nanotubes (MWCNTs) were obtained on Ni/Ce catalysts due to the formation of Ni–O–Ce solid solution in Ni/Ce catalysts, which improved the dispersion of Ni particles on the surface of the CeO_2 support, so that the Ni particles become small. The small-sized Ni particles become the active metal sites promoting the growth of MWCNTs and also the continuous decomposition of methane.

Gao *et al.*[60] prepared the bimetallic aerogel catalysts 9Ni–1Co/Al_2O_3 and 9Ni–1Co/Al_2O_3–TiO_2 catalysts (9Ni–1Co denotes the Ni and Co content in the catalysts were 9 and 1 wt. %, respectively, after the catalysts have been reduced) with a single support (Al_2O_3) and a composite support (TiO_2–Al_2O_3) using the sol-gel method. Experiments were carried out in a quartz fixed-bed reactor, and the methane conversions of the two types of catalysts were 69.3% and 72.5%, respectively, and the carbon produced was nanostructured. It was shown that the composite support formed by the addition of TiO_2 could improve the dispersion of the metal and enhance the activity of the carbon nanotube deposition sites, which was conducive to the transfer of carbon nanotubes off Ni and Co particles, and thus increased the utilization of Ni and Co particles and reduced the deactivation rate of the catalysts. The two aerogel catalysts still had high catalytic performance after two regeneration cycles.

Some experimental studies of hydrogen production from methane cracking catalyzed by nickel-based catalytic materials are summarized in Table I, and the main contents include reactor size, reaction conditions, maximum methane conversion, hydrogen yield, reaction duration, and solid carbon morphology.

In Table I, FB denotes the fixed-bed reactor, D_{in} denotes the internal diameter of the reactor (mm), L denotes the effective length of the reactor (mm), w is the weight of the catalyst used in the experiment (g), t is the required reaction time for methane to obtain the highest conversion (h), T is the experimental temperature of methane cracking (°C), F is the gas flow rate {a denotes the weight hourly space velocity [WHSV, ml/(gcat h)], i.e., the volume of gas passing over each gram of catalyst per hour; b denotes the gas flow rate (ml/min); c denotes the flow rate of gas in the standard state (ml/min)}, and X_{CH4}, X_{H2} are the maximum methane conversion and the maximum hydrogen yield during methane cracking, respectively, R_t denotes the total duration of the cracking reaction (h), CNTs are carbon nanotubes, CNFs are carbon nanofibers, GFs are graphene films, and CWNTs are multi-walled carbon nanotubes. The following formula calculated the methane conversion and hydrogen yield:

$$X_{CH4} = \frac{CH_{4_{in}} - CH_{4_{out}}}{CH_{4_{in}}} \times 100\%,$$

$$X_{H2} = \frac{H_{2_{out}}}{2CH_{4_{in}}} \times 100\%.$$

TABLE I. Characteristics of methane cracking over different nickel-based catalysts.

	FB reactor		Reaction condition				X_{CH4}	X_{H2}	R_t	
Catalysts	D_{in}	L	w	t	T	F	%	%	h	C morphology
Ni[50]	25	600	2	0.25	800	150[c]	···	65	6	C nano-chunks
Ni[50]	25	600	2	0.5	700	150[c]	···	55	6	C nano-chunks
Ni[50]	25	600	2	1	600	150[c]	···	40	6	C nano-chunks
50 at. %Ni/Al_2O_3[59]	15	1000	0.5	0.5	700	50[b]	···	45	6.5	CNFs + GFs
50 at. %Ni/CeO_2[59]	15	1000	0.5	0	700	50[b]	···	42	6.5	CWNTs
50Ni–15Pd/Al_2O_3[56]	10	700	0.05	0.5	750	12 000[a] (70 vol. % N_2)	90	···	10	CNFs
50Ni–20Pd/Al_2O_3[56]	10	700	0.05	0.5	750	12 000[a] (70 vol. % N_2)	85	···	10	CNFs
50Ni–10Fe/Al_2O_3[57]	10	700	0.05	1.5	750	12 000[a] (70 vol. % N_2)	70	···	10	CNFs
9Ni–1Co/Al_2O_3[60]	10	···	0.16	0	650	42 000[a] (70 vol. % N_2)	69.3	···	1.1	CNTs
50Ni–10Fe–10Cu/Al_2O_3[58]	10	700	0.05	1	750	12 000[a] (70 vol. % N_2)	83	···	10	CNFs
50Ni–10Fe–15Cu/Al_2O_3[58]	10	700	0.05	1	750	12 000[a] (70 vol. % N_2)	84	···	10	CNFs
Ni/CeO_2–Al_2O_3 (Ce:Al = 25:75 at. %)[59]	15	1000	0.5	2	700	50[b]	···	53	6.5	CNFs + GFs
Ni/CeO_2–Al_2O_3 (Ce:Al = 75:25 at. %)[59]	15	1000	0.5	2.5	700	50[b]	···	44	6.5	CNFs + GFs
9Ni–1Co/Al_2O_3–TiO_2[60]	10	···	0.16	0	650	42 000[a] (70 vol. % N_2)	72.5	···	1.1	CNTs

C. Iron-based catalysts

In addition to using nickel- and carbon-based materials as catalysts, many scholars have conducted studies with inexpensive iron-based materials for methane cracking. The iron-based catalytic materials can be categorized into ferroalloys, loaded monometallic iron, loaded ferroalloys, and natural iron ores. It has been found that methane can be completely catalyzed, and the catalyst has a long reaction life (>75 h) when using iron obtained by reduction at temperatures between 800 and 900 °C to catalyze methane cracking.[61] With Fe–Cu alloys as methane cracking catalysts, the generation of encapsulated carbon gives the Fe–Cu alloy catalysts better stability than the Raney-type (spongy pore structure) monometallic iron catalysts.[62]

Scholars have conducted more research using loaded iron-based catalysts. For example, alumina-based loaded iron-based catalysts (Fe_xO_y–Al_2O_3) were reduced to provide a ferrous oxide precursor with catalytically active sites, which had a significant impact on the stability and hydrogen yield of the catalysts due to the presence of Fe in the precursor in the +2 valence state, which facilitated its generation of catalytically active metallic iron in the subsequent reduction process.[63] The addition of the promoter Mo to Fe–MgO catalysts[64] significantly improved the catalytic performance, whereas adding Mo to the Fe–Al_2O_3 material was not as effective as the former.

Ni-, Fe-, and Co-based materials were loaded on MgO supports to generate bimetallic/MgO loaded-alloy catalysts,[65] with a total metal content of 50 wt. % after the catalysts were reduced. The results of experimental studies showed that the 25Fe–25Co/MgO catalysts (25Fe–25Co means that after the catalyst was reduced, the content of Fe and Co were both 25 wt. % of the catalyst) had high activity and stability. In contrast, the catalytic activity of both catalysts was significantly reduced by doping 25 wt. % Ni into 25Fe/MgO or 25Co/MgO. In addition, Fe–Co-based catalysts can achieve a higher yield of multi-walled nanotubes compared to Ni–Fe-based and Ni–Co-based catalysts, and the multi-walled nanotubes are highly graphitized and crystalline, which further proves that Fe–Co-based catalysts are more effective for the catalytic cracking of methane. In addition, it was also found that the catalytic performance of the 25Fe–25Co/MgO catalyst increased with reaction time, and the catalyst performance reached its highest after 5 h of reaction and maintained stability for a long time.

The catalyst 15Fe/$CeZrO_2$[66] was made by loading Fe on cerium–zirconium oxide supports (15Fe denotes a 15% mass fraction of Fe in the reduced catalyst), which showed a gradual increase in activity with the addition of Co or Mo. In the deactivated catalysts, phases such as graphitic carbon, Fe_3C, and Mo_2C was observed on both Fe- and Fe–Co-based alloy catalysts. The by-product carbon in the deactivated 15Fe/$CeZrO_2$ catalysts was mainly in the form of a coke structure, whereas in the deactivated catalysts with the addition of Co or Mo, the by-product carbon was mainly in the form of a nano-structure.

Al-Fatesh *et al.*[67] investigated the effectiveness of trimetallic alloy catalysts for catalytic cracking of methane with Fe-based materials as the main catalytic substance. Single, bimetallic, and trimetallic catalysts were prepared by loading materials containing Fe, Co, and Ni substances on alumina supports. It was found that 30 wt. % Fe–15wt. %Co/Al_2O_3 catalyst had the best performance. After 12 cycles of regeneration reaction (1400 min, with a reaction time of about 110 min for each cycle), the catalyst was still achievable a methane conversion of 55%.

On the other hand, Dai *et al.*[68] investigated the effect of doping Fe on the catalytic performance of La-containing catalysts. They prepared $LaFe_xAl_{12-x}O_{19}$ (x = 1 or 3) catalysts by the co-precipitation method, which had obvious hexaaluminate diffraction peaks because the increase in the Fe content was beneficial to increase the active center of the catalyst, so the catalytic activity of $LaFe_3Al_9O_{19}$ was higher than that of $LaFeAl_{11}O_{19}$. With $LaFe_3Al_9O_{19}$ as the methane cracking catalyst, the mixture (CH_4:air = 82.7:12.8) with a velocity of 18 cm/s was able to reach 888 °C in the reactor and finally achieved a methane conversion of 99.2%, and the gas produced by the device contained some CO.

In general, all solid catalysts for methane cracking require a synthesis step, which makes the hydrogen production process from methane cracking cumbersome. Exploiting cheap, abundant materials that require only simple processing for methane catalytic cracking is an important research direction in this field. Some scholars have investigated natural iron ores as catalysts for methane cracking. In 2018, Zhou *et al.*[69] used four natural iron ores with Fe_2O_3 contents ranging from 91.7% to 96.2% as methane cracking catalysts. The iron ores were milled to the particle size of 50 μm. Then, 1.6 g of catalyst was placed in a fluidized bed reactor with an inner diameter of 27 mm at 850 °C and 0.5 MPa with a flow rate of 100 ml/min of pure methane, resulting in a maximum methane conversion of about 78%. In the reacted catalyst, carbon was present as a mixture of Fe_3C and graphitic carbon with many pores, which was very influential in wastewater purification.

Silva *et al.*[33] investigated Tierga iron ore and ilmenite (52.6% and 33.3% of iron content, respectively) as cracking catalysts. Figure 4 demonstrates the effect of methane cracking over Tierga iron ore after being activated by H_2 or CH_4; it can be seen that the methane cracking can still achieve about 55% conversion after the reaction has been carried out for 3 h at 900 °C. On the catalyst after the reaction, the I_D/I_G value in the Raman spectrogram of the by-product carbon was less than 1 and around 0.2 (D-peak represents the defects in the lattice of C atoms, G-peak represents the stretching vibration in the sp2 hybrid plane of C atoms, I_D/I_G is the ratio of the intensities of the two peaks, which is used to indicate the degree of graphitization of the carbon, and the smaller the value of I_D/I_G, the higher the degree of crystallinity and the higher the ordering of the carbon), so that the by-products obtained were highly graphitized of carbon nanomaterials. Their study also found that, at the beginning of methane cracking, the catalytic cracking conversion reached 67% on Tierga iron ore but only up to 11% on ilmenite. Therefore, Tierga iron ore is also a good cracking catalyst for methane and is less costly than other iron-based catalysts.

In 2023, Dawkins *et al.*[70] investigated the effect of grinding time of iron ore on its activity in catalyzing the methane cracking and the carbon purity. The results showed that the optimum grinding time for iron ore was 270 min at a ball mill speed of 300 rpm, and the use of ball-milled iron ore as a catalyst resulted in a fivefold increase in methane conversion compared to unground ore. In addition to reducing the particle size of the ore and increasing its surface area, the grinding treatment caused a phase transition of the particles on the surface of the ore from magnetite to maghemite and hematite. However, prolonged ball milling does not consistently increase the surface area of the iron ore. Contrarily, excessive prolongation of the ball milling time leads to attachment of iron ore particles, which is not conducive to achieving maximum catalytic activity of the catalyst and higher methane conversion. In addition, the by-product carbon attached to the catalyst after the reaction is mainly high-purity carbon with a disordered

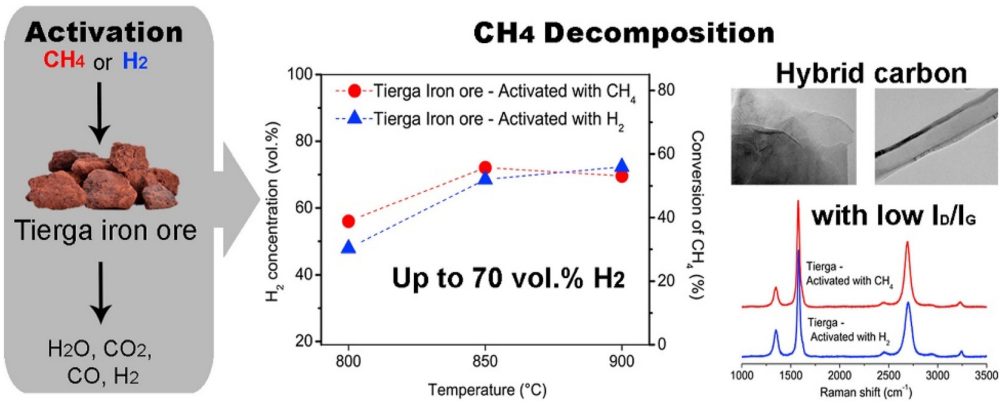

FIG. 4. Cracking of methane on Tierga iron ore.[33]

graphite structure, similar to low- to medium-quality metallurgical coke.

The experimental studies on hydrogen production from methane cracking catalyzed by iron-based catalytic materials are summarized in Table II, and the main contents include reactor type and size, reaction conditions, maximum methane conversion, hydrogen yield, reaction duration, and solid carbon morphology.

In this table, FB denotes fixed-bed reactor, RB denotes rotating-bed reactor, FIB denotes fluidized-bed reactor, D_{in} denotes the internal diameter of the reactor (mm), L denotes the effective length of the reactor (mm), w is the weight of the catalyst used for the experiment (g), t is the required reaction time for methane to obtain the highest conversion (g), T is the experimental temperature of methane cracking (°C), F is the gas flow rate {a denotes the weight hourly space velocity [WHSV, ml/(gcat h)], b denotes the gas flow rate (ml/min), c denotes the flow rate of gas in the standard state (ml/min)}, and X_{CH4}, X_{H2} are the highest methane conversion and the largest hydrogen yield during methane cracking. R_t denotes the total time (h) of the cracking reaction. CNTs are carbon nanotubes, CNFs are carbon nanofibers, and CWNTs are multi-walled carbon nanotubes.

III. MOLTEN MEDIA

The molten metal-catalyzed methane cracking process is based on solid catalyst-catalyzed methane cracking, in which the catalyst is

TABLE II. Characteristics of methane cracking with different iron-based catalysts.

	Reactor			Reaction condition				X_{CH4}	X_{H2}	R_t	
Catalysts	Type	D_{in}	L	w	t	T	F	%	%	h	C morphology
Fe[61]	FB	11	457	2	14	800	20[b]	98	···	>75	CNFs
Fe[56]	FB	25	600	2	0.4	800	150[c]	65	···	6	Graphene Sheets
50Fe–Cu[62]	FB	27	750	0.75	1.6	600	110[c]	51	···	5	CNFs
50Fe/Al_2O_3[71]	RB	65	800	···	0.4	800	1500[a]	···	90	3	CNFs + CNTs
Fe/Al_2O_3[72]	FIB	18	600	20	0	900	6000[a]	68	···	6	CNFs + CWNTs
20Fe/Al_2O_3[63]	FB	9.1	300	0.3	1.5	800	5000[a]	83	···	3	CNFs
60Fe/Al_2O_3[73]	FB	9.4	480	0.3	0.5	700	33[b] (9.1 vol. % N_2)	···	77.2	4	CNTs
67 mol. %Fe/MgO[64]	FB	18	600	0.15	0	800	2000[a]	···	55	3	CNFs
15Fe/$CeZrO_2$[66]	FB	9	762	1	0	1000	100[b] (95 vol. % N_2)	83	···	2.12	CNTs
15Fe–5Co/$CeZrO_2$[66]	FB	9	762	1	0	1000	100[b] (95 vol. % N_2)	89	···	2.12	Chain-like nano-C
15Fe–5Mo/$CeZrO_2$[66]	FB	9	762	1	0	1000	100[b] (95 vol. % N_2)	90	···	2.12	CNTs
30Fe–15Co/Al_2O_3[67]	FB	10	700	0.05	1	750	5000[a]	···	73	3	CNFs
50Ni–10Fe–15Cu/Al_2O_3[59]	FB	10	700	0.3	1	750	12 000[a] (70 vol. % N_2)	···	82	10	CNTs
25Fe–25Co/Al_2O_3[65]	FB	15	1000	0.5	5	700	50[b]	···	86	10	CNTs
50Fe–5Mo/MgO[71]	RB	65	800	···	0.4	800	1500[a]	···	91	3	CNFs
Iron ore[69]	FB	27	···	1.6	0	850	100[b]	78	···	10	Graphene C + Fe3C
Tierga ore[33]	FB	···	···	0.6	0.5	900	2000[a]	···	67	3	CNFs
Ilmenite[33]	FB	···	···	0.6	2	800	2000[a]	···	11	3	···

changed to a metal with a low melting point, which is then heated and melted in a reaction vessel.[7] Methane is blown through a pipe or nozzle into the high-temperature molten metal, which is subsequently cracked into hydrogen and carbon by the catalytic action of the melt. Due to the significant density difference between the solid carbon and the liquid metal, the generated carbon can be floated up to the liquid metal layer through buoyancy, and continuous separation is achieved in subsequent processes.[41] The cost of hydrogen production from methane cracking can be reduced if the carbon is purified and processed for sale as a high-value-added product. This process does not have the problem of solid catalyst being covered by carbon, carbon coking, or poisonous deactivation, so there is no need for the regeneration process of the failed catalyst, which avoids the problem of carbon in methane being transformed into CO_2.[42] In addition, the flowing liquid metal has high thermal conductivity, which helps to provide stable heat for the methane cracking process, so that the melt temperature will not fluctuate significantly during the methane cracking process, ensuring production stability.[74]

In addition, molten salts can remain single-phase liquids at high temperatures; they have better thermal conductivity and insulation properties than molten metals.[75] Moreover, the contact angle between molten salt and carbon is larger compared to that between molten metal and carbon,[76,77] so the carbon generated from the cracking of methane in molten salt has less liquid entrapped when it floats upward, which reduces the loss of the melt, and thus, molten salts are also widely used in the hydrogen production process of catalytic methane cracking. Figure 5 shows a typical molten media catalytic methane cracking device and catalytic cracking process.

Although the use of molten media avoids the problem of conversion of carbon in methane to CO_2, scholars have found some problems with the process in their studies. First, the catalytic methane cracking effect is not good; for example, when Palmer *et al.*[78] catalyzed methane cracking at 950 °C using a bubble column reactor with a molten Ni_{27}–Bi_{73} alloy, the residence time of methane in the melt is 1 s, and the conversion was less than 10%. Zeng *et al.*[79] melted tellurium which a high

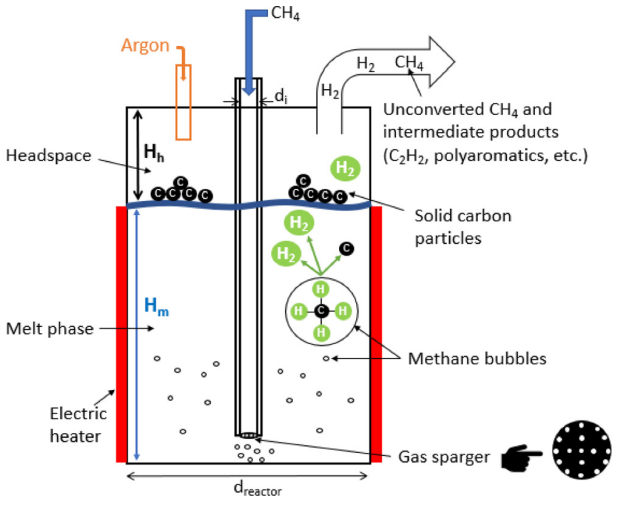

FIG. 5. Conventional molten media catalytic methane cracking unit with catalytic cracking process.[42]

electron affinity at 827 °C–977 °C, the methane has a residence time of 12 s, and the conversion was only 30%. Second, the by-product carbon has low purity due to the entrapment of metals and also causes the problem of high metal consumption. Rahimi[80] found that the by-product carbon recovered from a molten Ni–Bi single-phase reactor contained 83 wt. % of metals. Zaghloul[81] also found that stacked carbon particles entrapped tin metal, resulting in low purity and high metal loss.

Therefore, compared with the solid catalyst catalyzed methane cracking process, the low cracking conversion of methane in molten medium, the low purity of carbon, and the difficulty of purifying carbon at a later stage are the problems that need to be solved in this process.

A. Molten monometallic catalysts

Considering the cost and simplicity of the process, scholars would like to use low melting point metals as catalysts for methane cracking. Previous researchers found that nickel, platinum, palladium, cobalt, and iron metal elements have high melting points[82] and require a large amount of heat when melting into a liquid state. Wang *et al.*[83] found that magnesium can also catalyze methane cracking. However, magnesium has a lower boiling point and is volatile, and using magnesium as a melting medium to catalyze methane cracking increases the amount of metal loss.

Although metallic elements such as indium, gallium, tin, lead, and bismuth are weak catalysts for methane cracking reactions,[84] because of the advantage of low melting points (e.g., the melting points of gallium, tin, and bismuth are 30, 232, and 271 °C, respectively[85]), these metals became the preferred choice of scholars to be used in the study of the melting medium catalyzed methane cracking process in the early days.

Regarding the choice of reactors, Serban *et al.*[86] proposed to use the heat generated by a Generation IV nuclear reactor in direct contact with molten metal Sn to heat it to the pyrolysis temperature of methane, where methane is catalytically cracked to hydrogen and carbon. A Mott sprayer sprayed methane into the Sn medium at 750 °C, and 51% methane conversion was obtained, corresponding to the output of 70 vol. % H_2. This study showed that methane conversion is mainly affected by the contact time between methane, the heat transfer medium, and the size of the methane bubbles. The Mott sprayer effectively decreased the size of the methane bubbles, leading to increased methane conversion. Kudinov *et al.*[87] applied numerical calculations and experiments to study the cracking reaction of methane in molten Sn. The increase in methane flow rate from 25 to 250 ml/min resulted in an increase in the diameter of the bubbles and a faster rise speed. The rapid rise of the bubbles caused the contact time between the bubbles and the liquid to decrease, decreasing the output hydrogen from 12 to 4.4 vol. %. The authors suggested placing cascading mesh spacers in the reactor, which reduced the methane bubble size and extends the contact time between the bubbles and the liquids. Msheik *et al.*[88] used a novel hybrid solar/electric bubble reactor (the melt is Sn) to investigate methane pyrolysis. Their results showed that the size of the bubbles has an essential effect on the methane conversion because the small bubbles can significantly increase the residence time of the bubble in the melt and improve the heat transfer effect. So, finding a suitable catalytic liquid medium or generating small bubbles via suitable spargers is still challenging.

Agar *et al.*[89] investigated carbon deposition in a fluid wall flow reactor and a molten metal capillary reactor. The fluid wall flow reactor, shown in Fig. 6, is based on the principle of heat transfer by passing heated inert gas through porous ceramic tubes into the pyrolysis zone using convective heat transfer. The heated helium gas enters the reaction zone through a 3 μm membrane reactor to provide heat, and the reaction is carried out for 7 h. The methane conversion decreased from 53% to 7%, remaining constant after that. The results showed that carbon deposition from the decomposition of methane diffusing into the heated zone cannot be avoided. So, the fluid wall flow reactor is unsuitable for continuous methane pyrolysis. Figure 7 shows the formation of blocking flow in a capillary reactor, where T-joints are used to generate the blocking flow, water is introduced from the top, and nitrogen is blown in from the left side. The alternating bubbles and blocking streams form a liquid film at the capillary wall, which not only avoids carbon deposition but also prolongs the residence time of the bubbles. Methane was passed into the molten Sn at a speed of 0.122 m/s to enable continuous cracking reactions, realizing an average methane conversion of 32%, and no carbon deposition occurred. To address the issues of carbon deposition, gas separation, and instability of the blocking flow, the team performed hydrodynamic characterization with Ga, In, Sn, and alloys of these metals,[90] and using various types of gases to establish a stable blocking flow. In addition, the reaction system was updated, but increasing the residence time of the bubbles by extending the capillary reactor requires higher pressures and influences the device's viability.

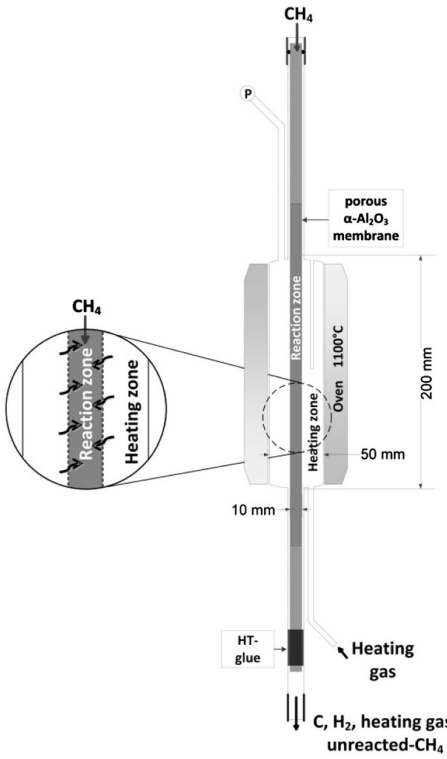

FIG. 6. Fluid wall flow reactor unit.[89] Reproduced with permission from Schultz and Agar, Int. J. Hydrogen Energy **40**, 11422–11427 (2015). Copyright 2015 Elsevier Ltd.

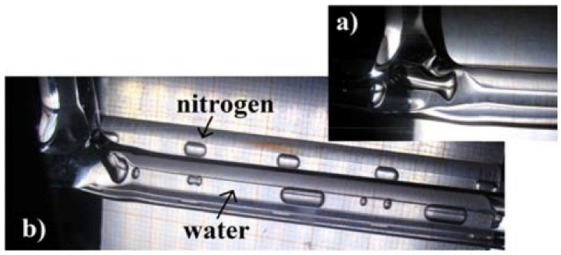

FIG. 7. The process of formation of blocking flow:[89] (a) blockage flow generated at the T-joints; and (b) blockage flow within the reaction zone. Reproduced with permission from Schultz and Agar, Int. J. Hydrogen Energy **40**, 11422–11427 (2015). Copyright 2015 Elsevier Ltd.

Regarding the catalytic properties of low melting point metals, Plevan *et al.*[91] found that the experimental data for methane conversion in melted Sn were lower than the model predictions when the temperature was in the range of 700–950 °C. Therefore, it is concluded that molten Sn has no catalytic effect on the cracking reaction of methane, but it can reduce the amount of intermediates, such as ethane and ethylene. To improve the conversion of methane in molten Sn, the team of Geißler[92,93] fluxed methane at a rate of 50 ml/min into molten Sn at 1000 °C, and achieved a hydrogen production rate of 30 vol. %; the gas products generated were examined and found to be composed mainly of methane and hydrogen, with only a small amount of intermediate gases (∼1.5 mol. %). With a constant methane flow rate and a melt Sn temperature of 1175 °C, the hydrogen yield was as high as 78%, and the results indicated that increasing the melt temperature improves the methane conversion significantly.

Zeng *et al.*[79] used elemental tellurium, which has high electron affinity, as a melt catalyst for the methane cracking reaction. As the temperature approached the boiling point of tellurium, tellurium volatilized into the gaseous state. It was found that gaseous tellurium was also a catalyst for the methane cracking reaction, but the catalytic efficiency was not as good as that of liquid tellurium. In addition, the authors found that the addition of metallic nickel to molten tellurium reduced its catalytic activity. The experimental method and results of liquid/gaseous tellurium catalyzed methane cracking are illustrated in Fig. 8. Wi *et al.*[94] investigated the catalytic effect of five molten pure metals (indium, gallium, bismuth, tin, and copper) on the cracking of

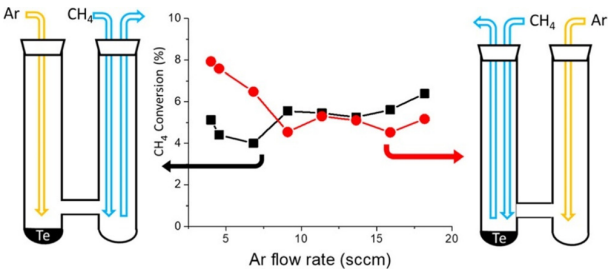

FIG. 8. Experimental methods and results of methane cracking in molten and gaseous tellurium.[79] Reprinted with permission from Zeng *et al.*, ACS Catal. **10**, 8223–8230 (2020). Copyright 2020 American Chemical Society.

methane by using the electromagnetic levitation technique. The results showed that the maximum rate of methane cracking reaction in molten Bi was observed at 1100 °C, while below 1000 °C, the maximum rate of methane cracking reaction was observed in molten Ga. When the catalytic performance of metals is reflected by the rate constant of catalytic reaction (k_f), the product of k_f and A_M is inversely proportional to the first ionization energy of the metal catalyst (A_M is the molar surface area of the metal catalyst; and the first ionization energy is the energy required for the gaseous atoms in the ground state to lose one of their outermost electrons, with the smaller value being the more prone to lose electrons).

Leal Pérez *et al.*[74] used low-melting gallium as a catalyst and heat transfer agent for methane cracking. Methane was blown into a quartz-tube bubble column reactor from a porous plate distributor when the melt temperature was 1119 °C, and the bubble residence time was only 0.5 s, but the conversion reached 91%. Due to the high heat storage capability of gallium [specific heat capacity about 2.26 J/(cm^3 K)], it ensures a more homogeneous temperature profile for the reaction. Temperature homogeneity can improve methane conversion, so suitable temperature control at the industrial scale concept is important. However, gallium metal is too expensive and not suitable for industrial production.

B. Molten alloy catalysts

Although the melting temperature of low-melting-point metals is low, it is found from the above study that in order to achieve an excellent cracking effect, the temperature of the molten metal has to reach about 1000 °C, which is already much higher than the melting point of low-melting-point metals. Moreover, low-melting-point metals are inferior to high-melting-point metals such as nickel, iron, and cobalt in terms of catalytic performance. When weak catalytic metal elements are added to catalytic metals as carriers, the two can generate low melting point alloys with sound catalytic effects.

In 2017, Upham *et al.*[82] catalyzed the cracking of methane using a bubbling reaction column (1100 mm) containing a molten $Ni_{27}Bi_{73}$ alloy, which resulted in a methane conversion of 95% when the melt temperature was 1065 °C and the exit gas was pure hydrogen with no detectable CO_2 or other by-product gases. The by-product carbon was graphite with a purity of 92 at. %. When the melt temperature was lowered to 1040 °C, the methane conversion decreased to 84%, and in addition, the melt stability exceeded 170 h. The alloy was considered to be the best melt catalyst for methane cracking discovered at that time. They used thermostatic first-principles molecular dynamics simulations to calculate the electronic properties of the alloy melt. They found that Ni was present in the melt as partially negatively charged atoms, so the catalytic performance was considered to be related to the amount of charge on the Ni atoms.

The following year, Palmer *et al.*[95] were surprised that molten $Cu_{45}Bi_{55}$ alloys catalyzed methane cracking better than molten $Ni_{23}Bi_{73}$ alloys. Although metallic copper and bismuth are weak catalysts for methane cracking, their molten alloys showed a good catalytic cracking effect. The results of surface tension experiments and thermostatic first-principles molecular dynamics simulations of the structure and chemistry of the molten $Cu_{45}Bi_{55}$ alloys showed that the surface of the molten alloys was enriched with Bi atoms that lacked electrons (Bi lacks electrons because it provides electrons to Cu, which is negatively charged), and these Bi atoms became the active sites for methane activation. So, the Bi atoms lacking electrons promoted the dissociation of methane due to the coordination of Bi with CH_3^* free radicals, which allowed the H atoms to combine with the negatively charged Cu atoms, thus breaking the C–H bond. Hence, the $Cu_{45}Bi_{55}$ alloy had a good methane-catalyzed cracking effect, but the methane conversion and the stability of the alloy were not reported in their article.

Scheiblehner *et al.*[96] investigated the effect of catalytic cracking of methane by copper-containing binary alloy melts (CuBi, CuSn, CuNi, and CuGa). The methane gas was blown at a 50 ml/min flow rate from an alumina lance into a reactor with an inner diameter of 65 mm, a melt height of 70 mm, and a melt temperature of 1160 °C. The results showed that the molten $Cu_{20}Bi_{80}$ alloys have the lowest surface tension, and methane has the highest conversion of 68.44% in these melts. Theoretical and simulation calculations showed that adding Bi, Sn, or Ga in the Cu melt decreases the surface tension of the melt and the size of the bubbles formed at the lance, which has some positive effects on methane conversion.

Regarding the improvement of the molten alloy catalytic cracking methane reactor, Kim *et al.*[97] sprayed methane from a quartz tube with an inner diameter of 2 mm and a ceramic sprayer at the bottom into a reactor (inner diameter 12 mm, height 500 mm, melt filling height 110 mm) containing a molten alloy of $Ni_{20}Sn_{80}$ at 1000 °C. The highest conversion of methane could reach 97%, and graphitic carbon was produced. Their homemade ceramic porous distributor successfully reduced the bubble size from a range of 3–8 mm (no sprayer) to 0.5 mm and finally increased methane conversion. The main material of the ceramic sprayer is zirconia; the surface of the sprayer provides active sites for the catalyst melt, and the active Ni is dispersed on the surface of the sprayer, which promotes further methane cracking. When the methane gas was blown directly into the reactor from a quartz tube without the ceramic sprayer, the methane conversion was only 15%–25%, and the resulting graphitic carbon was defective and disordered.

In 2023, Chen *et al.*[98] discovered a catalyst that was simple to prepare and had high performance, which is Ni–Mo–Bi (mass ratio of each element is 2.3:1.3:96.4) ternary molten alloy, which enables the catalytic methane cracking reaction temperature down to 800 °C. The cracking activation energy of methane with this catalyst at 800 °C was 81.2 kJ/mol, close to its cracking activation energy in solid metal catalysts (65–90 kJ/mol). At an ambient pressure of 206 kPa, methane was blown into the molten alloy catalyst at a 4 ml/min flow rate. The residence time of methane bubbles in the alloy was about 7.8 s. The generation rate of H_2 reached 4.05 ml/(gNi min), which is 37 times higher than that in the Ni–Bi alloy [0.11 ml/(gNi min)], and the intermediates such as acetylene and aromatic compounds were not detected in the gaseous products. In addition, the reaction stability of the Ni–Mo–Bi ternary molten alloy could reach 120 h. The reason why the Ni–Mo–Bi ternary molten alloy showed superior catalytic cracking performance than that of Ni–Bi alloy is that the introduction of Mo into the Ni–Bi molten alloy enhanced the strong interaction between Ni and Mo, which regulated the electronic valence state of Ni and led to the reduction of the negative charge of Ni and the decrease in the interaction between Ni and Bi, increasing the mobility of the active metal Ni in the solvent Bi at the same time.

C. Molten salt catalysts

In the floating process of the carbon generated from methane cracking in molten metal, there will be severe carbon contamination

due to the entrapped metal, and this problem is a common problem in the catalytic cracking of methane by molten metal or alloy. To solve the problem, some scholars proposed using molten salts with low wettability with carbon.

In 2019, Kang *et al.*[99] used a KCl–$MnCl_2$ (67:33 mol. %) mixture as a molten catalyst, and methane was cracked in a liquid-column bubbling reactor at 700 to 1050 °C. The results showed that the apparent activation energy of methane cracking decreased to 161 kJ/mol, the methane conversion reached 30%, and the by-product carbon was graphitic. By washing the carbon with water, they reduced the salt entrapped to less than 7 at. %. In the following year, they used $FeCl_3$(3 wt. %)–NaCl–KCl as a catalyst,[100] and the activation energy of methane cracking decreased from 301 kJ/mol (no $FeCl_3$) to 171 kJ/mol, and the reactivity life of this molten salt was more than 50 h. The authors speculated that the presence of Fe^{3+} activated the C–H bond. The by-product carbon, on the other hand, was flaky graphite, and the purity of the carbon ranged from 92.83 ± 2.61 at. %. Boo *et al.*[101] used a single KCl molten salt to catalyze methane cracking, and the apparent activation energy was calculated to be 277 ± 15 kJ/mol. The molten salt continued to demonstrate good stability for 40 h. The by-product carbon was treated with water washing, hydrochloric acid cleaning, and ultrasonic waves and then heated in an argon atmosphere at 1200 °C to obtain the highest carbon purity, up to 97.2 at. %. The authors analyzed the economics of the process and concluded that it could compete with the SMR process using CCS when the loss of molten salts is minimized, and the gain of carbon is maximized.

Parkinson *et al.*[102] used halide molten salts [NaBr, KBr, KCl, NaCl, NaBr–KBr (48.7:51.3 mol. %)] for the catalytic cracking of methane. The activation energies of methane cracking in these molten salts ranged from 223.5 to 277.6 kJ/mol. Although the carbon still entraps many molten salts to float to the liquid surface, the carbon purity can reach 91.7–97.4 at. % after washing with de-ionized water. In addition, the by-product carbon has the properties of low density (<1 g/cm^3), high porosity (30.1–75.2%), small specific surface area (1.84–3.14 m^2/g), and relatively low ordered structure.

Although the purity of by-product carbon obtained from methane cracking in molten salts is improved, the conversion of methane in single-phase molten salts is not high because molten salts are not strong catalysts for methane cracking, and this drawback makes the method of catalytic cracking of methane in single-phase molten salts unworkable. In order to obtain both high-purity carbon by-products and high methane conversion, the researchers developed a two-phase liquid reactor with molten metal and molten salt, where the lower molten metal layer is mainly used to improve methane cracking conversion, and the upper molten salt layer is used to clean the carbon.

Rahimi *et al.*[80] investigated methane cracking in a two-phase reactor with molten Ni–Bi alloy and (NaBr/KBr) molten salt. The metal content of the carbon produced in the two-phase reactor was less than 5 at. %, and the carbon was subsequently purified to less than 2 at. % of the molten salt, and no metals were detected. Second, the content of contaminants in solid carbon decreased with increasing height of the molten salt layer, and it concluded that the bubbles ruptured as they rose into the molten salt phase, and the metal droplets carried by the bubbles flowed back into the alloy phase. In addition, since the bromide (NaBr/KBr) molten salt has a high affinity for carbon, the metal around the carbon was replaced by the molten salt, which detached from the carbon surface and returned to the metal phase.

Noh *et al.*[103] performed catalytic cracking experiments on methane using a NiBi–ZrO_2–NaBr 3-stage bubble column reactor. At 985 °C, the methane conversion increased from 32% (2-stage bubble column reactor) to 37%, and the carbon purity was increased from 70 to 74 wt. %. The catalyst system still showed good stability after 50 h of reaction. Figure 9 shows Noh's 3-stage bubble column reactor setup.

Parkinson *et al.*[104] added molten NaBr–KBr (48.7:51.3 mol. %) with γ-Al_2O_3 suspended catalyst particles in a bubbling reactor for methane cracking, and the device was used to investigate the rate of catalyzed cracking of methane at 850–1000 °C. Using a double U-bend injector in the reactor reduced the rising speed of methane bubbles in the melt. It thus extended their residence time and significantly increased the methane conversion. When the height of the molten

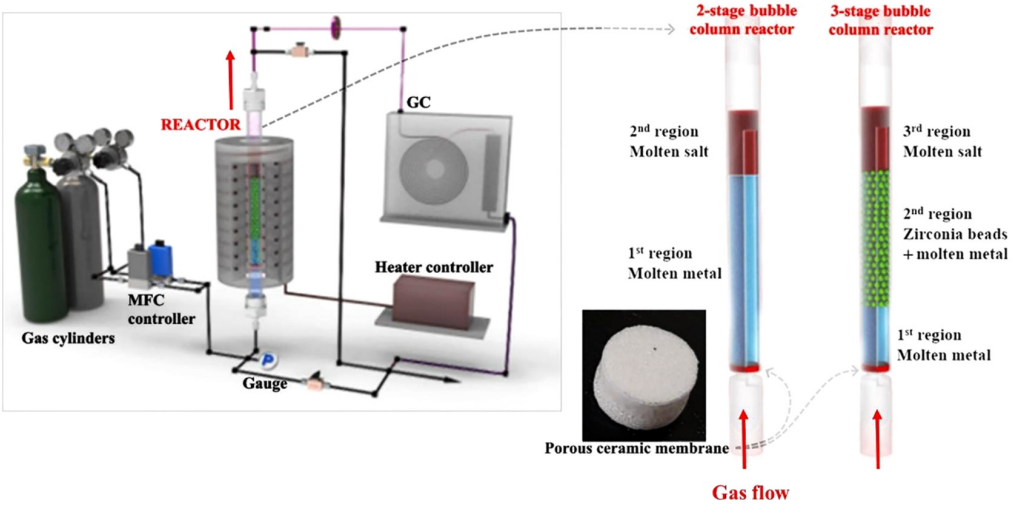

FIG. 9. NiBi–ZrO_2–NaBr 3-stage bubble column reactor setup.[103] Reproduced with permission from Noh *et al.*, Chem. Eng. J. **428**, 131095 (2022). Copyright 2022 Elsevier.

alloy was 190 mm, and the content of γ-Al_2O_3 particles was increased from 0 to 5 wt. %, the cracking activation energy of methane decreased from 246.9 to 128.4 kJ/mol, implying that the presence of the particles in the melt enhanced the mass transfer rate at the interface. When the concentration of particles increased to 1.25 wt. %, the decreasing trend of the apparent activation energy of methane cracking leveled off, indicating that the diffusion rate of methane at the bubble interface became the limiting step for the cracking reaction at this time.

Additionally, they replaced the γ-Al_2O_3 particles with Co–Mn catalyst particles.[105] The results showed that the Co–Mn catalyst particles prolonged the cracking time of methane in the melt at 1000 °C. There was no disintegration, abrasion, or dissolution of Co–Mn particles in the 24-h experiments, and stable hydrogen yields could be achieved. Increasing the molar ratio of Co/Mn in the particles also increased the conversion of CH_4. The addition of suspended particles to the molten salt can only be used for mechanistic studies of the methane cracking process and is not applicable in actual production because of the buildup of solidified molten salt and particles in the detachment zone in the upper layer of the molten salt, which can cause clogging and pressure buildup in the reactor over a long period of operation.

Table III summarizes the experimental conditions and main results of methane cracking in different molten media.

In Table II, D_{in} denotes the internal diameter of the reactor (mm), H denotes the height of the reactor (mm), D_{end} is the size of the end of the gas injector (mm), L denotes the effective filling height of the catalyst medium in the reactor (mm), t denotes the residence time of the gas bubbles in the medium (s), T denotes the experimental temperature of methane cracking (°C), F is the rate of the gas flow [b denotes the flow rate of the gas (ml/min), c denotes the flow rate of gas in the standard condition (ml/min)], and X_{CH4} denotes the highest methane conversion during methane cracking.

D. Summary of methane cracking in molten media

The method of molten metal catalyzed methane cracking has the following advantages: (1) there is no problem of poisoning and

TABLE III. Comparison of test results of catalytic methane cracking in molten media.

	Reactor			Reaction condition				X_{CH4}	C purity	C
Molten medium	D_{in}	H	D_{end}	L	t	T	F	%	%	morphology
Sn[91]	35.9	1150	1	1000	1.7–2.7	900	5[b]	18	···	···
Sn[93]	40.6	1268	0.5	250	3.2–4.9	1000	50[c]	···	30	C Soot
Sn[86]	25.4	355.6	0.0005	101.6	0.3–0.5	750	15[b]	51	···	C Soot + graphite
Sn[106]	3	500	1	120	···	1300	500[c] (70 vol. % Ar)	64	···	C powder+ C sheets
Mg[83]	16	200	3	15	···	700	5[b]	<30	···	C Soot
Te[79]	12	>400	···	70	<12	750	10[b] (30 vol. % Ar)	>30	Te > 2 at. %	Disordered graphic C
Ga[74]	36	360	0.16–0.25	150	0.5	1119	450[c] (50 vol. % Ar)	91	···	C black
$Ni_{27}Bi_{73}$[82]	30	···	···	1100	7	1065	10[b] (10 vol. % Ar)	95	···	graphite
$Ni_{27}Bi_{73}$–NaBr[80]	22	···	2	660 + 260	5.3	1000	10[b]	37.5	>95 wt. %	C clack + CNTs
$Ni_{27}Bi_{73}$–NaBr[103]	8	650	>0.01	65 + 31	···	985	9[b] (33 vol. % Ar)	···	70 wt. %	Disordered graphic C
$MnCl_2$–KCl (67:33 mol. %)[99]	25	250	2	125	0.6	1050	5[b]	55	>96 at. %	graphic sheets
NaCl–KCl (1.02:1mol. %)–$FeCl_3$ (3 wt. %)[100]	25	250	2	125	0.6	1000	20[b]	9	>92.8 at. %	graphic sheets
NaBr–KBr (48.7:51.3 mol. %)[102]	16	250	2	190	0.69–0.76	1000	15[b]	5.85	91.7–97.4 at. %	Disordered nano-C
NaBr–KBr (48.7:51.3 mol. %)–Al_2O_3 (2.5 wt. %)[104]	26	700	2	580	10	1000	45[b] (67 vol. % Ar)	···	···	Disordered nano-C
$Ni_{27}Bi_{73}$–ZrO_2–NaBr[103]	8	650	>0.01	48 + 38 + 31	···	985	9[b] (33 vol. % Ar)	···	74 wt. %	Disordered graphic C+ little C fiber

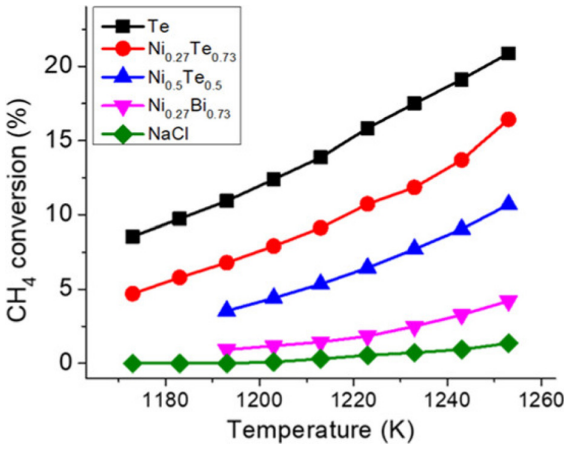

FIG. 10. Conversion ratios of methane cracking in different molten media.[79] Reprinted with permission from Zeng *et al.*, ACS Catal. **10**, 8223–8230 (2020). Copyright 2020 American Chemical Society.

deactivation of the catalyst by carbon covering and coking, and the carbon in methane is not emitted as a gas. (2) Continuous separation of product hydrogen and carbon can be realized in the production process, ensuring the continuity and stability of actual production. (3) If the by-product carbon is processed to make high-value-added carbon materials for sale, some of the production costs of the process can be scaled down. (4) Solid carbon is more accessible to collect and store than gaseous CO_2, and since the SMR hydrogen production process emits a large amount of CO_2, the molten metal catalyzed methane cracking process can compete with the current SMR process applied for large-scale production when the capture and storage of CO_2 is considered.[92,107]

Different molten media catalyze methane cracking with different properties. In general, molten alloys have the best catalytic effect, next are molten metals, and molten salts are last.[82] However, metal Te is an exception,[79] as seen in Fig. 10, tellurium activity decreases upon the addition of Ni to the melt; the reason may be that those specific electronic interactions between Te and Ni reduce the concentration of tellurium in contact with methane. Furthermore, we can find that the catalytic effect increases with the increase in temperature, which means that high temperature is an indispensable condition to obtain a good methane conversion in molten metal.

Although molten salts are weak catalysts for methane cracking reactions, they have the following advantages over molten metals: (1) Molten salts have a lower density and require less mass than molten metals to fill the same reactor volume, reducing their cost.[108] (2) By-product carbon of methane cracking in molten salts can be cleaned to achieve higher purity, and it is easier to remove molten salts than metal from carbon. (3) The lower vapor pressure of the molten salt not only reduces its evaporation during the cracking process of methane but also reduces the amount of melt loss in a reactor with more than two phases, where the upper molten salt inhibits the evaporation of the lower metal.[42]

Because there are more advantages of the molten media catalytic cracking methane for hydrogen production, many researchers have done many works on this zone, and the main development trend of molten media is shown in Fig. 11. It can be found that the catalytic performance of metal is related to its electronegativity.[109] Different catalysts have advantages and disadvantages, as molten alloys have good catalytic effects but contaminate by-product carbon, and molten salts can purify carbon but are weak catalysts. The future molten catalysts will be a multiphase liquid medium combined with molten alloy and molten salt to achieve high methane conversion and low carbon pollution.

Hydrogen production from methane by catalytic cracking in molten media has many advantages and is a novel and low-carbon emission process. With the emergence of high-quality catalysts (e.g., NiBi, CuBi, NiMoBi, etc.) and two-phase molten media reactors for purifying carbon, methane cracking in molten media will most likely become a new trend. However, the choice of the medium as the cracking catalyst for methane in the actual production process still needs to be more conclusive, and researchers must conduct more in-depth fundamental research and industrial studies gradually to promote the catalytic cracking methane to hydrogen in molten media into the industrialization stage.

IV. MECHANISTIC ANALYSIS OF METHANE CRACKING

The reaction of catalytic cracking of methane is generally divided into three steps: (1) methane gas diffuses to the catalyst surface and adsorbs on the catalyst surface; (2) methane gas is activated by the catalyst to reduce the C–H bonding energy, followed by the cracking

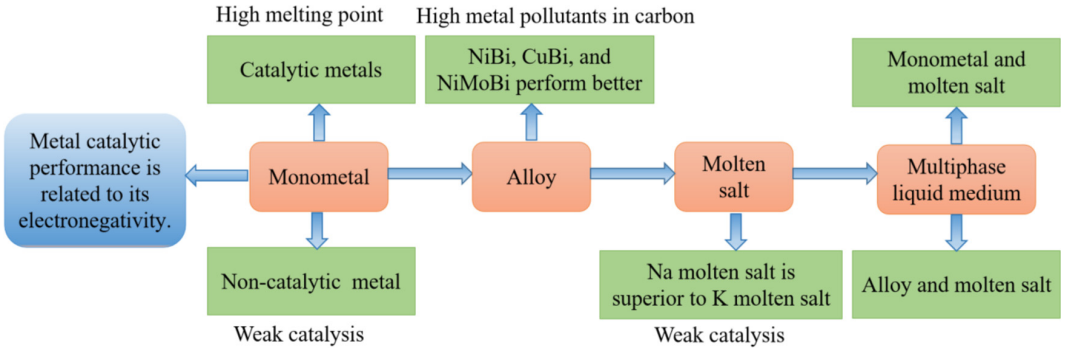

FIG. 11. The development trend of molten media for methane cracking.

reaction to generate hydrogen and solid carbon; and (3) generated hydrogen is desorbed from the catalyst surface and diffuses into the gas phase. Only by deeply analyzing and fully understanding the mechanism and kinetics of the methane cracking process can we grasp the correct research direction of the rapid methane cracking reaction for hydrogen production.

In the 1970s, Chen[110,111] investigated the cracking mechanism of methane in different static systems at temperatures of 722, 765, 795, and 830 °C, pressures in the range of 0.0033–0.0933 MPa. It was found that methane cracking produced intermediate gas products such as ethane, ethylene, and acetylene in addition to hydrogen. The cracking process of methane is described by the homogeneous, nonchain radical mechanism:

$$CH_4 \rightarrow CH_3\cdot + H\cdot, \quad (1)$$

$$H\cdot + CH_4 \rightarrow CH_3\cdot + H_2, \quad (2)$$

$$2CH_3\cdot \rightarrow C_2H_6, \quad (3)$$

$$CH_3\cdot + C_2H_6 \rightarrow CH_4 + C_2H_5\cdot, \quad (4)$$

$$C_2H_5\cdot \rightarrow C_2H_4 + H\cdot. \quad (5)$$

In terms of melt-catalyzed cracking, Wang *et al.*[83] proposed a possible pathway for the cracking reaction of hydrocarbons on molten magnesium metal (Fig. 12). Molten magnesium can transfer heat to the decomposition process in addition to activating the C–H bonds of hydrocarbons. Cracking of hydrocarbons produces not only hydrogen but also Mg_2C_3 and Mg_2C intermediates. Due to the instability of magnesium carbide, it tends to decompose into carbon and magnesium, after which the magnesium is returned to the reaction system, and the carbon is separated and removed.

Isotope exchange experiments between CH_4 and D_2 (D is an isotope of H) in pure KCl by Palmer *et al.*[112] showed that the dehydrogenation order of methane is $CH_3D > CH_2D_2 > CHD_3 > CD_4$, indicating that pure KCl activated the first C–H bond of CH_4 to produce CH_3^*. Based on the density functional theory and molecular dynamics simulation, Bae *et al.*[113] simulated the isotope exchange experiments of CH_4–D_2 in the melts of $MnCl_2$, KCl, and $MnCl_2$–KCl mixtures. The results showed that more CH_2D_2 and CH_3D deuterium products existed on the surface of the molten salts of $MnCl_2$ than that of KCl, so it is believed that pure $MnCl_2$ contains catalytic activator,

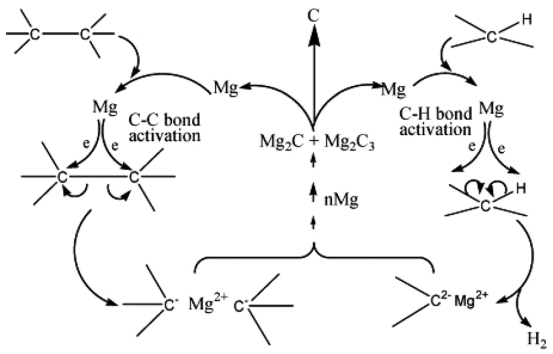

FIG. 12. Hydrocarbon pyrolysis path in molten magnesium.[83] Reproduced with permission from Wang *et al.*, J. Mol. Catal. A **283**, 153–157 (2008). Copyright 2008 Elsevier BV.

which is favorable for the breaking of the first C–H bond in methane, and the formation of CH_3^* is promoted. However, the critical step in the cracking reaction of methane is still the generation of CH_3^*. In addition, the density functional theory calculations and experiments confirmed that the cracking of methane in $MnCl_2$–KCl mixed molten salt produces a large amount of CH_2^*, and the possible reason is that the energy barrier for the transition from CH_3^* to CH_2^* in the mixed molten salt is low, so the catalytic system has a unique pathway of methane dehydrogenation. The mixed molten salt of $MnCl_2$–KCl is more active in catalyzing methane cracking than the pure $MnCl_2$ and KCl.

Kang *et al.*[100] found in their experiments on methane cracking catalyzed by $FeCl_3$–NaCl–KCl molten salts that the apparent activation energy of methane cracking decreased from 301 kJ/mol (0 Fe) to 171 kJ/mol (3 wt. % $FeCl_3$) with an increase in the concentration of $FeCl_3$, the apparent first-order rate exponent decreased at the same time, which was consistent with a transition from a gas-phase collision-based reaction pathway to a surface-mediated catalytic process. In addition, where CHD_3 and CH_2D_2 were generated in large quantities, the mixtures CH_4 and D_2 underwent H–D exchange reactions, contributing to methane cracking.

The Arrhenius plots obtained by Palmer *et al.*[95] in their experiments on methane cracking catalyzed by molten $Cu_{45}Bi_{55}$ confirmed it as a first-order reaction. The surface tension of the alloy was measured by the maximum bubble pressure method, and it was found that a small amount of Bi was present in the solvent Cu, so the surface tension of Cu was lowered so that Bi would be enriched on the surface of Cu, then Cu absorbs methane better. Scholars used constant-temperature *ab initio* molecular dynamics to simulate the methane cracking process; the results are shown in Fig. 13. The path of methane dissociation to generate the CH_3–Bi bond and H–Cu bond requires the lowest energy, that is, the methane dissociation process to generate methyl bismuth and copper hydride is more stable. Hence, the presence of Bi promotes the cracking of methane.

In addition, Palmer *et al.*[95] applied the nudged elastic band method (NEB) to study the dissociation energies of H and CH_3^* when they are most stable on the surface of the $Cu_{45}Bi_{55}$ melt. The results are shown in Fig. 14. It was shown that the activation energies of methane cracking in the two stable states were 2.53 and 2.60 eV, which were very close to each other and close to the experimentally measured effective activation energy of 2.3 ± 0.2 eV. From this, the final dissociation energies of methane in the two stable states were obtained as +1.22 and +1.25 eV, respectively.

V. CHARACTERIZATION OF BY-PROCUCT CARBON

One of the advantages of molten-metal cracking is that the by-product carbon can be continuously separated and collected from the melt, and the competitiveness of molten-metal-catalyzed methane cracking for hydrogen production can be improved if the carbon is processed and purified to be sold as a high-value-added material. Carbon materials with different properties are sold at different prices in the market, e.g., carbon black is sold at 0.34–1.92 USD/kg, graphitic carbon is sold at about 9.04 USD/kg, and carbon fibers are sold in the range of 22.59–106.19 USD/kg.[114] The morphological characteristics of the by-product carbon are related to the catalyst and operating conditions used in the methane cracking process, and it is reported that higher methane dilution rates cause the formation of larger carbon particles during methane cracking.[93] The cracking of methane molecules in the melt differs from conventional thermal cracking and catalytic

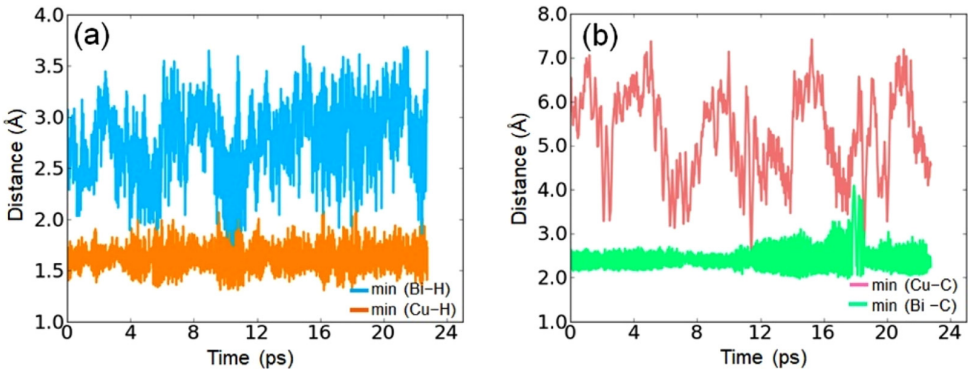

FIG. 13. Shortest distances of H or C from Bi or Cu atoms, respectively, on the surface of the molten $Cu_{45}Bi_{55}$.[95] (a) shortest distance between Bi or Cu atoms and H, and (b) shortest distance between Bi or Cu atoms and C. Reprinted with permission from Palmer *et al.*, ACS Catal. **9**, 8337–8345 (2019). Copyright 2019 American Chemical Society.

cracking with solid catalysts. The dissolution process of carbon atoms generated by the decomposition of methane in the melt hinders the growth of nanofibers and nanotubes. Section V outlines the morphological characteristics of the by-product carbon generated from the catalytic methane cracking with molten media.

First, the by-product carbon of methane cracking in molten metal has different structures depending on the medium. The carbon produced by catalytic cracking in molten Te is disordered,[79] and the carbon produced in molten Ga is carbon black.[74] Most of the carbon generated by the cracking of methane in the melts Sn, $SnCu_5$, and $SnNi_5$ was stacked,[81] while in the melt $SnCu_{30}$, a tubular structure of carbon was found; in addition, all the carbon generated was partially entrained with metallic Sn. The presence of Ni in the melt reduces the amorphous structure of the carbon and moves the carbon toward a graphitized structure.

The purity of carbon obtained in molten salts will be much higher. The cracking of methane in NaCl–KCl molten salts gave carbon a spherical structure. After adding 3 wt. % of $FeCl_3$ into the molten salts, the carbon was obtained as a polycrystalline flake graphite structure, with the final purity exceeding 90 at. %.[100] The carbon obtained from methane cracking in $MnCl_2$–KCl molten salt showed a polycrystalline flake graphite structure with a size of about 11 nm. In contrast, the carbon produced in pure $MnCl_2$ molten salt showed an irregular amorphous structure with large particles.[99]

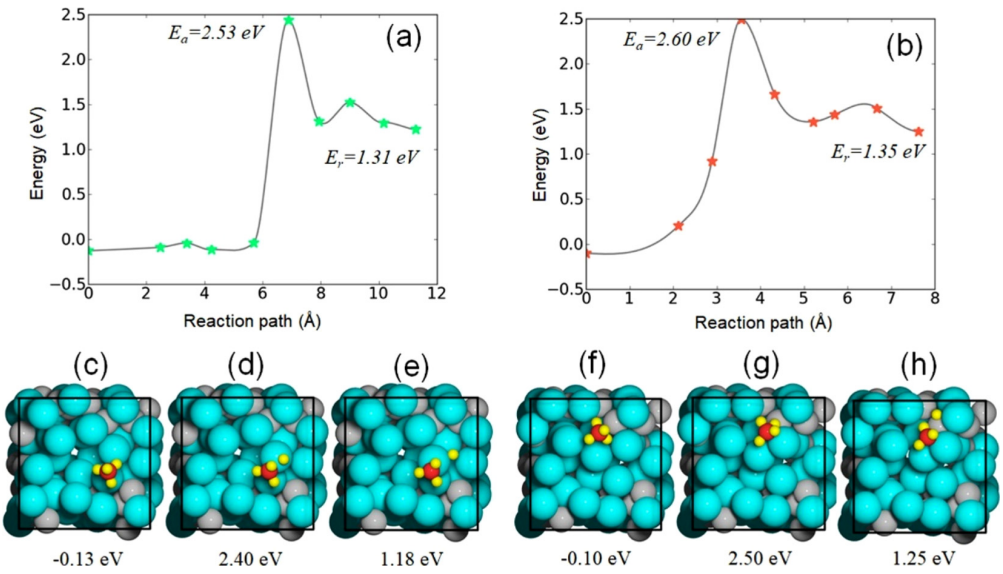

FIG. 14. Energy changes of methane dissociation process on molten $Cu_{45}Bi_{55}$ surfaces.[95] (a) Both CH_3^* and H are placed on the Bi atom. (b) CH_3^* is on the Bi atom, and H is between two Cu atoms. (c) and (f) Initial state of arrangement of atoms on the surface of the melt and dissociation energy of methane. (d) and (g) Arrangement of atoms on the surface of the melt during methane dissociation and dissociation energy of methane. (e) and (h) Dissociated state of methane consisting of CH_3^* and H. Reprinted with permission from Palmer *et al.*, ACS Catal. **9**, 8337–8345 (2019). Copyright 2019 American Chemical Society.

Rahimi *et al.*[80] found that methane cracked in a single-phase NiBi melt yielded carbon flakes of graphitic carbon, whereas most of the particles of carbon generated by cracking in a two-phase NiBi–NaBr/KBr melt were 20–50 nm spheres and a few aggregates of 100–200 nm carbon black. In addition, KBr has a more substantial wetting effect on carbon, so it is more likely to be entrapped by carbon and become a contaminant of carbon, so the purity of carbon generated in the upper layer of NaBr molten salt will be higher than that of carbon generated in the upper layer of KBr molten salt.

VI. SUMMARY AND PROSPECT

Green and clean hydrogen energy is getting more and more attention as the Earth faces the severe problem of climate warming. As a result, the demand for hydrogen is rising in society. The method of methane cracking for hydrogen production is considered an ideal process because the by-product carbon exists in a solid form. However, the process needs to be more mature for production practice. This paper comprehensively reviews the catalytic properties, cracking mechanism, and by-product carbon morphology in the methane cracking process for hydrogen production. We want to find a suitable pathway for the hydrogen production process.

First, this paper reviews the experimental studies on carbon-based and nickel-based materials as methane-cracking catalysts. All solid catalytic materials suffer from the problem of deactivation due to carbon coverage and thus face the challenge of emitting a large amount of greenhouse gases when the failed catalysts are regenerated. Adding some Fe or Ni catalytic metals to carbon-based catalysts can improve the catalytic activity of carbon-based materials. When nickel-based materials are used as catalysts, the catalytic cracking temperature of methane can be lowered to less than 800 °C, and methane has a perfect cracking effect on nickel-based catalysts, so nickel-based catalysts are still attracting the attention of many researchers. However, the problem of high susceptibility to deactivation of nickel-based catalysts is a priority that needs to be solved urgently.

Second, this paper comprehensively summarizes the study of using iron-based catalysts. The catalytic performance of iron-based materials is slightly inferior to nickel-based materials but still shows an excellent catalytic cracking effect. In addition, since cheap iron ore powder catalysts do not require a synthesis step, they can be used for the catalytic cracking of methane after simple grinding. It has been reported that iron ore catalytic cracking of methane can achieve 78% methane conversion. As a methane-cracking catalyst, iron ore powder demonstrates significant cost and catalytic effect advantages. Since iron ore is an abundant resource, the devitalized ore powder can be further utilized as raw material for ironmaking, avoiding the catalyst regeneration problem.

Third, a detailed review of experiments on methane cracking in molten metals, molten alloys, molten salts, and two-phase liquid media is presented. Methane cracking in molten metals or alloys typically has higher conversion than in molten salts, but carbon contamination is severe. The new study found that Cu–Bi alloys are better than Ni–Bi alloys for the catalytic cracking of methane because the H atoms in methane are prone to bond with Cu atoms, and Bi will be coordinated to CH_3^* radicals, which will activate and break the C–H bond in methane. In addition, the hydrogen production rate of methane cracking in Ni–Mo–Bi ternary alloy is 37 times higher than that of Ni–Bi alloy, and the stability of the reaction reaches 120 h. The purity of by-product carbon will significantly improve when it passes through the upper molten salt, and the carbon purity can reach more than 92 at. % after the carbon is washed by subsequent processing.

Fourth, the mechanism of methane cracking is analyzed. The cracking process of methane generates intermediate products such as ethane, ethylene, acetylene, etc. The dehydrogenation process of methane is carried out step by step, and the activation and breaking of the C–H bond is the crucial step to catalyze methane cracking. With the help of numerical simulation software, the microscopic process of methane cracking can be shown more clearly. However, the mechanism of methane cracking may change under different experimental conditions, and more detailed studies are needed to understand the mechanism in depth.

Finally, the structures of by-product carbon produced by methane cracking in molten metals are reviewed. Most of the by-product carbon generated from methane cracking in molten metals exists as carbon black. In contrast, the carbon generated in a single molten salt moves toward a graphitic structure.

The following research suggestions are put forward to obtain a stable and highly active catalyst for methane cracking and promote the industrialization of catalytic methane cracking hydrogen production.

1. It is necessary to combine experimental results with DFT calculation to identify the active center during methane conversion, reveal the real reaction process, and then clarify the reaction mechanism. In addition, *in situ* characterization techniques, such as x-ray photoelectron spectroscopy, x-ray diffraction, and transmission electron microscopy, should be used to observe the intermediates. This will provide important guidance for the design of high-performance catalysts.
2. The formation mechanism of carbon allotrope in the liquid phase catalytic system is still unclear and needs further study. Understanding the formation mechanism of by-products can clarify the production method of carbon products so that the molten media catalytic methane cracking technology can produce two valuable products.
3. The methane pyrolysis process requires heat, and burning fossil fuels to provide energy will emit greenhouse gases, so a new molten media solar reactor will become a new research direction of clean hydrogen production technology.
4. In addition to basic research, more efforts are needed to promote methane cracking to produce hydrogen for industrial applications. Therefore, it is indispensable to design and build large catalytic reactors to verify the activity and durability of industrial catalysts. Moreover, economic and technical analysis is also required to determine the technical feasibility of methane cracking for hydrogen production.

ACKNOWLEDGMENTS

This research was funded by the National Key R&D Program Project of China Minmetals Corporation (Grant No. 2022YFC2906100) and the China Minmetals Science and Technology Project of China Minmetals Corporation (Grant No. 2020ZXA01).

AUTHOR DECLARATIONS

Conflict of Interest

The authors have no conflicts to disclose.

Author Contributions

Lei Guo: Conceptualization (equal); Funding acquisition (equal); Project administration (lead); Supervision (lead); Writing – review & editing (lead). **Jinchi Tan:** Conceptualization (equal); Investigation (equal); Project administration (equal); Validation (equal); Writing – original draft (equal); Writing – review & editing (equal). **Junyue Ren:** Investigation (supporting); Resources (equal); Writing – original draft (equal). **Zhancheng Guo:** Funding acquisition (equal); Project administration (equal); Validation (equal); Writing – review & editing (equal).

DATA AVAILABILITY

The data that support the findings of this study are available within the article.

REFERENCES

[1]X. Duan, J. Xu, Z. Wei *et al.*, "Metal-free carbon materials for CO_2 electrochemical reduction," Adv. Mater. **29**, 1701784 (2017).
[2]Y. Song, X. Zhang, K. Xie *et al.*, "High-temperature CO_2 electrolysis in solid oxide electrolysis cells: developments, challenges, and prospects," Adv. Mater. **31**, 1902033 (2019).
[3]J. F. Dean, "Old methane and modern climate change. Old methane is less important for our immediate future than contemporary sources," Science **367**, 846–848 (2020).
[4]H. Dotan, A. Landman, S. W. Sheehan *et al.*, "Decoupled hydrogen and oxygen evolution by a two-step electrochemical-chemical cycle for efficient overall water splitting," Nat. Energy **4**, 786–795 (2019).
[5]S. Stephens-Romero, M. Carreras-Sospedra, J. Brouwer *et al.*, "Determining air quality and greenhouse gas impacts of hydrogen infrastructure and fuel cell vehicles," Environ. Sci. Technol. **43**, 9022–9029 (2009).
[6]Q. Li, X. Lin, Q. Luo, Y. Chen *et al.*, "Kinetics of the hydrogen absorption and desorption processes of hydrogen storage alloys: A review," Int. J. Miner., Metall. Mater. **29**, 32–48 (2022).
[7]Z. Fan, W. Weng, J. Zhou *et al.*, "Catalytic decomposition of methane to produce hydrogen: A review," J. Energy Chem. **58**, 415–430 (2021).
[8]J. Tang, M.-s. Chu, F. Li *et al.*, "Development and progress on hydrogen metallurgy," Int. J. Miner. Metall. Mater. **27**, 713–723 (2020).
[9]J. Zhang, J. Schenk, Z. Liu *et al.*, "Editorial for special issue on hydrogen metallurgy," Int. J. Miner. Metall. **29**, 1817–1819 (2022).
[10]M. G. Rasul, M. A. Hazrat, M. A. Sattar *et al.*, "The future of hydrogen: Challenges on production, storage and applications," Energy Convers. Manage. **272**, 116326 (2022).
[11]W. N. A. W. Yusoff, N. A. Baharuddin, M. R. Somalu *et al.*, "Recent advances and influencing parameters in developing electrode materials for symmetrical solid oxide fuel cells," Int. J. Miner. Metall. Mater. **30**, 1933–1956 (2023).
[12]A. Atkinson, S. Barnett, R. J. Gorte *et al.*, "Advanced anodes for high-temperature fuel cells," Nat. Mater. **3**, 17–27 (2004).
[13]J. Song, Z. Zhao, X. Zhao *et al.*, "Hydrogen storage properties of MgH_2 co-catalyzed by LaH_3 and NbH," Int. J. Miner. Metall. Mater. **24**, 1183–1191 (2017).
[14]F. M. Nyahuma, L. Zhang, M. Song *et al.*, "Significantly improved hydrogen storage behaviors in MgH_2 with Nb nanocatalyst," Int. J. Miner. Metall. Mater. **29**, 1788–1797 (2022).
[15]N. Xu, Z. Yuan, Z. Ma *et al.*, "Effects of highly dispersed Ni nanoparticles on the hydrogen storage performance of MgH_2," Int. J. Miner. Metall. Mater. **30**, 54–62 (2023).
[16]J. Zhang, B. Zhang, X. Xie *et al.*, "Recent advances in the nanoconfinement of Mg-related hydrogen storage materials: A minor review," Int. J. Miner. Metall. Mater. **30**, 14–24 (2023).
[17]Y. He, L. Zhu, L. Li *et al.*, "Hydrogen and power cogeneration based on chemical looping combustion: Is it capable of reducing carbon emissions and the cost of production?," Energy Fuels **34**, 3501–3512 (2020).
[18]A. S. Damle, "Hydrogen production by reforming of liquid hydrocarbons in a membrane reactor for portable power generation—Experimental studies," J. Power Sources **186**, 167–177 (2009).
[19]X. Liu, G. Liu, J. Xue *et al.*, "Hydrogen as a carrier of renewable energies toward carbon neutrality: State-of-the-art and challenging issues," Int. J. Miner. Metall. Mater. **29**, 1073–1089 (2022).
[20]R. G. Lemus and J. M. Martínez Duar, "Updated hydrogen production costs and parities for conventional and renewable technologies," Int. J. Hydrogen Energy **35**, 3929–3936 (2010).
[21]S. Abanades and G. Flamant, "Experimental study and modeling of a high-temperature solar chemical reactor for hydrogen production from methane cracking," Int. J. Hydrogen Energy **32**, 1508–1515 (2007).
[22]D. Paxman, S. Trottier, M. Nikoo *et al.*, "Initial experimental and theoretical investigation of solar molten media methane cracking for hydrogen production," Energy Procedia **49**, 2027–2036 (2014).
[23]P. H. J. Conti, J. Diefenderfer, A. LaRose *et al.*, in *International Energy Outlook 2016 With Projections to 2040* [USDOE Energy Information Administration (EIA), Office of Energy Analysis, Washington, DC, 2016].
[24]B. Parkinson, P. Balcombe, J. F. Speirs *et al.*, "Levelized cost of CO_2 mitigation from hydrogen production routes," Energy Environ. Sci. **12**, 19–40 (2019).
[25]N. Muradov, F. Smith, C. Huang, and A. T-Raissi, "Autothermal catalytic pyrolysis of methane as a new route to hydrogen production with reduced CO_2 emissions," Catal. Today **116**, 281–288 (2006).
[26]M. J. Lázaro, J. L. Pinilla, R. Utrilla *et al.*, "H_2–CH_4 mixtures produced by carbon-catalyzed methane decomposition as a fuel for internal combustion engines," Energy Fuels **24**, 3340–3345 (2010).
[27]E. K. Lee, S. Y. Lee, G. Y. Han *et al.*, "Catalytic decomposition of methane over carbon blacks for CO_2-free hydrogen production," Carbon **42**, 2641–2648 (2004).
[28]I. Suelves, M. J. Lázaro, R. Moliner, J. L. Pinilla *et al.*, "Hydrogen production by methane decarbonization: Carbonaceous catalysts," Int. J. Hydrogen Energy **32**, 3320–3326 (2007).
[29]S. Kazemi, S. M. Alavi, and M. Rezaei, "Influence of various spinel materials supported Ni catalysts on thermocatalytic decomposition of methane for the production of CO_x-free hydrogen," Fuel Process. Technol. **240**, 107575 (2023).
[30]Y. Echegoyen, I. Suelves, M. J. Lázaro *et al.*, "Hydrogen production by thermocatalytic decomposition of methane over Ni-Al and Ni-Cu-Al catalysts: Effect of calcination temperature," J. Power Sources **169**, 150–157 (2007).
[31]M. A. Ermakova, D. Y. Ermakov, and G. G. Kuvshinov, "Effective catalysts for direct cracking of methane to produce hydrogen and filamentous carbon: Part I. Nickel catalysts," Appl. Catal., A **201**, 61–70 (2000).
[32]T. Zhang and M. D. Amiridis, "Hydrogen production via the direct cracking of methane over silica-supported nickel catalysts," Appl. Catal., A **167**, 161–172 (1998).
[33]J. Alves Silva, J. B. Oliveira Santos, D. Torres *et al.*, "Natural Fe-based catalysts for the production of hydrogen and carbon nanomaterials via methane decomposition," Int. J. Hydrogen Energy **46**, 35137–35148 (2021).
[34]P. Forzatti and L. Lietti, "Catalyst deactivation," Catal. Today **52**, 165–181 (1999).
[35]C. H. Bartholomew, "Mechanisms of catalyst deactivation," Appl. Catal. A-Gen. **212**, 17–60 (2001).
[36]H. F. Abbas and W. M. A. W. Daud, "Thermocatalytic decomposition of methane for hydrogen production using activated carbon catalyst: Regeneration and characterization studies," Int. J. Hydrogen Energy **34**, 8034–8045 (2009).
[37]U. P. M. Ashik, W. M. A. Wan Daud, and H. F. Abbas, "Production of greenhouse gas free hydrogen by thermocatalytic decomposition of methane—A review," Renewable Sustainable Energy Rev. **44**, 221–256 (2015).
[38]R. Y. Kannah, S. Kavitha, Preethi *et al.*, "Techno-economic assessment of various hydrogen production methods—A review," Bioresour. Technol. **319**, 124175 (2021).
[39]H. F. Abbas and W. M. A. Wan Daud, "Hydrogen production by methane decomposition: A review," Int. J. Hydrogen Energy **35**, 1160–1190 (2010).
[40]J. Raza, A. H. Khoja, M. Anwar *et al.*, "Methane decomposition for hydrogen production: A comprehensive review on catalyst selection and reactor systems," Renewable Sustainable Energy Rev. **168**, 112774 (2022).

[41]M. McConnachie, M. Konarova, and S. Smart, "Literature review of the catalytic pyrolysis of methane for hydrogen and carbon production," Int. J. Hydrogen Energy **48**, 25660–25682 (2023).
[42]M. Msheik, S. Rodat, and S. Abanades, "Methane cracking for hydrogen production: A review of catalytic and molten media pyrolysis," Energies **14**, 3107 (2021).
[43]J. L. Pinilla, I. Suelves, R. Utrilla *et al.*, "Hydrogen production by thermocatalytic decomposition of methane regeneration of active carbons using CO_2," J. Power Sources **169**, 103–109 (2007).
[44]K. Harun, S. Adhikari, and H. Jahromi, "Hydrogen production via thermocatalytic decomposition of methane using carbon-based catalysts," RSC Adv. **10**, 40882–40893 (2020).
[45]J. Wang, L. Jin, Y. Li, and H. Hu, "Preparation of Fe-doped carbon catalyst for methane decomposition to hydrogen," Ind. Eng. Chem. Res. **56**, 11021–11027 (2017).
[46]J. Zhang, L. Jin, Y. Li *et al.*, "Hierarchical porous carbon catalyst for simultaneous preparation of hydrogen and fibrous carbon by catalytic methane decomposition," Int. J. Hydrogen Energy **38**, 8732–8740 (2013).
[47]F. Liu, L. Yang, and C. Song, "Chemical looping hydrogen production using activated carbon and carbon black as multi-function carriers," Int. J. Hydrogen Energy **43**, 5501–5511 (2018).
[48]D. P. Serrano, J. A. Botas, and R. Guil-Lopez, "H_2 production from methane pyrolysis over commercial carbon catalysts: Kinetic and deactivation study," Int. J. Hydrogen Energy **34**, 4488–4494 (2009).
[49]K. Srilatha, V. Viditha, D. Srinivasulu *et al.*, "Hydrogen production using thermocatalytic decomposition of methane on Ni_{30}/activated carbon and Ni_{30}/carbon black," Environ. Sci. Pollut. Res. **23**, 9303–9311 (2016).
[50]M. Pudukudy, A. Kadier, Z. Yaakob, and M. S. Takriff, "Non-oxidative thermocatalytic decomposition of methane into CO_x free hydrogen and nanocarbon over unsupported porous NiO and Fe_2O_3 catalysts," Int. J. Hydrogen Energy **41**, 18509–18521 (2016).
[51]L. Zhou and J. M. Basset, "Unsupported NiPt alloy metal catalysts prepared by water-in-oil (W/O) microemulsion method for methane cracking," Fuel **181**, 805–810 (2016).
[52]A. Venugopal, S. Naveen Kumar, J. Ashok *et al.*, "Hydrogen production by catalytic decomposition of methane over Ni/SiO_2," Int. J. Hydrogen Energy **32**, 1782–1788 (2007).
[53]S. Takenaka, Y. Shigeta, E. Tanabe, and K. Otsuka, "Methane decomposition into hydrogen and carbon nanofibers over supported Pd–Ni catalysts," J. Catal. **220**, 468–477 (2003).
[54]J. I. Villacampa, C. Royo, E. Romeo *et al.*, "Catalytic decomposition of methane over Ni-Al_2O_3 coprecipitated catalysts. Reaction and regeneration studies," Appl. Catal., A **252**, 363–383 (2003).
[55]A. M. Amin, E. Croiset, C. Constantinou, and W. Epling, "Methane cracking using Ni supported on porous and non-porous alumina catalysts," Int. J. Hydrogen Energy **37**, 9038–9048 (2012).
[56]N. Bayat, M. Rezaei, and F. Meshkani, "Hydrogen and carbon nanofibers synthesis by methane decomposition over Ni-Pd/Al_2O_3 catalyst," Int. J. Hydrogen Energy **41**, 5494–5503 (2016).
[57]N. Bayat, M. Rezaei, and F. Meshkani, "Methane decomposition over Ni–Fe/Al_2O_3 catalysts for production of CO_x-free hydrogen and carbon nanofiber," Int. J. Hydrogen Energy **41**, 1574–1584 (2016).
[58]N. Bayat, F. Meshkani, and M. Rezaei, "Thermocatalytic decomposition of methane to CO_x-free hydrogen and carbon over Ni-Fe-Cu/Al_2O_3 catalysts," Int. J. Hydrogen Energy **41**, 13039–13049 (2016).
[59]W. Ahmed, A. E. Awadallah, and A. A. Aboul-Enein, "Ni/CeO_2-Al_2O_3 catalysts for methane thermo-catalytic decomposition to CO_x-free H_2 production," Int. J. Hydrogen Energy **41**, 18484–18493 (2016).
[60]B. Gao, I. W. Wang, L. Ren, and J. Hu, "Catalytic methane decomposition over bimetallic transition metals supported on composite aerogel," Energy Fuels **33**, 9099–9106 (2019).
[61]A. Konieczny, K. Mondal, T. Wiltowski, and P. Dydo, "Catalyst development for thermocatalytic decomposition of methane to hydrogen," Int. J. Hydrogen Energy **33**, 264–272 (2008).
[62]A. F. Cunha, J. J. M. Órfão, and J. L. Figueiredo, "Methane decomposition on Fe-Cu Raney-type catalysts," Fuel Process. Technol. **90**, 1234–1240 (2009).
[63]A. H. Fakeeha, A. A. Ibrahim, W. U. Khan *et al.*, "Hydrogen production via catalytic methane decomposition over alumina supported iron catalyst," Arabian J. Chem. **11**, 405–414 (2018).
[64]J. L. Pinilla, R. Utrilla, R. K. Karn *et al.*, "High temperature iron-based catalysts for hydrogen and nanostructured carbon production by methane decomposition," Int. J. Hydrogen Energy **36**, 7832–7843 (2011).
[65]A. E. Awadallah, A. A. Aboul-Enein, D. S. El-Desouki *et al.*, "Catalytic thermal decomposition of methane to CO_x-free hydrogen and carbon nanotubes over MgO supported bimetallic group VIII catalysts," Appl. Surf. **296**, 100–107 (2014).
[66]V. Ramasubramanian, H. Ramsurn, and G. L. Price, "Hydrogen production by catalytic decomposition of methane over Fe based bi-metallic catalysts supported on CeO_2-ZrO_2," Int. J. Hydrogen Energy **45**, 12026–12036 (2020).
[67]A. S. Al-Fatesh, A. H. Fakeeha, W. U. Khan *et al.*, "Production of hydrogen by catalytic methane decomposition over alumina supported mono-, bi- and trimetallic catalysts," Int. J. Hydrogen Energy **41**, 22932–22940 (2016).
[68]H. Dai, Z. Song, H. Wang, and Q. Cui, "Efficient production of hydrogen by catalytic decomposition of methane with Fe-substituted Efficient production of hydrogen by catalytic decomposition of methane with Fe-substituted hexaaluminate coated packed bed," Energy **273**, 127272 (2023).
[69]L. Zhou, L. R. Enakonda, S. Li *et al.*, "Iron ore catalysts for methane decomposition to make CO_x free hydrogen and carbon nano material," J. Taiwan Inst. Chem. E **87**, 54–63 (2018).
[70]M. Dawkins, D. Saal, J. F. Marco *et al.*, "An iron ore-based catalyst for producing hydrogen and metallurgical carbon via catalytic methane pyrolysis for decarbonization of the steel industry," Int. J. Hydrogen Energy **48**, 21765–21777 (2023).
[71]J. L. Pinilla, R. Utrilla, M. J. Lázaro *et al.*, "Ni- and Fe-based catalysts for hydrogen and carbon nanofilament production by catalytic decomposition of methane in a rotary bed reactor," Fuel Process. Technol. **92**, 1480–1488 (2011).
[72]D. Torres, S. Llobet, J. L. Pinilla *et al.*, "Hydrogen production by catalytic decomposition of methane using a Fe-based catalyst in a fluidized bed reactor," J. Nat. Gas Chem. **21**, 367–373 (2012).
[73]A. A. Ibrahim, A. H. Fakeeha, A. S. Al-Fatesh *et al.*, "Methane decomposition over iron catalyst for hydrogen production," Int. J. Hydrogen Energy **40**, 7593–7600 (2015).
[74]B. J. Leal Pérez, J. A. Medrano Jiménez, R. Bhardwaj *et al.*, "Methane pyrolysis in a molten gallium bubble column reactor for sustainable hydrogen production: Proof of concept & techno-economic assessment," Int. J. Hydrogen Energy **46**, 4917–4935 (2021).
[75]R. Roper, M. Harkema, P. Sabharwall *et al.*, "Molten salt for advanced energy applications: A review," Ann. Nucl. Energy **169**, 108924 (2022).
[76]P. Baumli and G. Kaptay, "Wettability of carbon surfaces by pure molten alkali chlorides and their penetration into a porous graphite substrate," Mater. Sci. Eng., A **495**, 192–196 (2008).
[77]F. Wei, "Research status of liquid metal wetting on graphite surface," Gansu Sci. Technol. **35**, 32–35 (2019) (in Chinese).
[78]C. Palmer, E. Bunyan, J. Gelinas *et al.*, "CO_2-free hydrogen production by catalytic pyrolysis of hydrocarbon feedstocks in molten Ni-Bi," Energy Fuels **34**, 16073–16080 (2020).
[79]J. Zeng, M. Tarazkar, T. Pennebaker *et al.*, "Catalytic methane pyrolysis with liquid and vapor phase tellurium," ACS Catal. **10**, 8223–8230 (2020).
[80]N. Rahimi, D. Kang, J. Gelinas *et al.*, "Solid carbon production and recovery from high temperature methane pyrolysis in bubble columns containing molten metals and molten salts," Carbon **151**, 181–191 (2019).
[81]N. Zaghloul, S. Kodama, and H. Sekiguchi, "Hydrogen production by methane pyrolysis in a molten-metal bubble column," Chem. Eng. Technol. **44**, 1986–1993 (2021).
[82]D. C. Upham, V. Agarwal, A. Khechfe *et al.*, "Catalytic molten metals for the direct conversion of methane to hydrogen and separable carbon," Science **358**, 917–921 (2017).
[83]K. Wang, W. S. Li, and X. P. Zhou, "Hydrogen generation by direct decomposition of hydrocarbons over molten magnesium," J. Mol. Catal. A **283**, 153–157 (2008).
[84]R. Aiello, J. E. Fiscus, H.-C. zur Loye *et al.*, "Hydrogen production via the direct cracking of methane over Ni/SiO_2: Catalyst deactivation and regeneration," Appl. Catal., A **192**, 227–234 (2000).

[85]See https://ptable.com/#Properties for "Periodic Table-Ptable."
[86]M. Serban, M. A. Lewis, C. L. Marshall *et al.*, "Hydrogen production by direct contact pyrolysis of natural gas," Energy Fuels **17**, 705–713 (2003).
[87]I. V. Kudinov, A. A. Pimenov, Y. A. Kryukov *et al.*, "A theoretical and experimental study on hydrodynamics, heat exchange and diffusion during methane pyrolysis in a layer of molten tin," Int. J. Hydrogen Energy **46**, 10183–10190 (2021).
[88]M. Msheik, S. Rodat, and S. Abanades, "Enhancing molten tin methane pyrolysis performance for hydrogen and carbon production in a hybrid solar/electric bubbling reactor," Int. J. Hydrogen Energy **49**, 962–980 (2024).
[89]I. Schultz and D. W. Agar, "Decarbonisation of fossil energy via methane pyrolysis using two reactor concepts: Fluid wall flow reactor and molten metal capillary reactor," Int. J. Hydrogen Energy **40**, 11422–11427 (2015).
[90]A. A. Munera Parra and D. W. Agar, "Molten metal capillary reactor for the high-temperature pyrolysis of methane," Int. J. Hydrogen Energy **42**, 13641–13648 (2017).
[91]M. Plevan, T. Geißler, A. Abánades *et al.*, "Thermal cracking of methane in a liquid metal bubble column reactor: Experiments and kinetic analysis," Int. J. Hydrogen Energy **40**, 8020–8033 (2015).
[92]T. Geißler, A. Abánades, A. Heinzel *et al.*, "Hydrogen production via methane pyrolysis in a liquid metal bubble column reactor with a packed bed," Chem. Eng. J. **299**, 192–200 (2016).
[93]T. Geißler, M. Plevan, A. Abánades *et al.*, "Experimental investigation and thermochemical modeling of methane pyrolysis in a liquid metal bubble column reactor with a packed bed," Int. J. Hydrogen Energy **40**, 14134–14146 (2015).
[94]T.-G. Wi, Y.-J. Park, U. Lee, and Y.-B. Kang, "Methane pyrolysis rate measurement using electromagnetic levitation techniques for turquoise hydrogen production: Liquid In, Ga, Bi, Sn, and Cu as catalysts," Chem. Eng. J. **460**, 141558 (2023).
[95]C. Palmer, M. Tarazkar, H. H. Kristoffersen *et al.*, "Methane pyrolysis with a molten Cu-Bi alloy catalyst," ACS Catal. **9**, 8337–8345 (2019).
[96]D. Scheiblehner, D. Neuschitzer, S. Wibner *et al.*, "Hydrogen production by methane pyrolysis in molten binary copper alloys," Int. J. Hydrogen Energy **48**, 6233–6243 (2023).
[97]J. Kim, C. Oh, H. Oh *et al.*, "Catalytic methane pyrolysis for simultaneous production of hydrogen and graphitic carbon using a ceramic sparger in a molten NiSn alloy," Carbon **207**, 1–12 (2023).
[98]L. Chen, Z. Song, S. Zhang *et al.*, "Ternary NiMo-Bi liquid alloy catalyst for efficient hydrogen production from methane pyrolysis," Science **381**, 857–861 (2023).
[99]D. Kang, N. Rahimi, M. J. Gordon *et al.*, "Catalytic methane pyrolysis in molten $MnCl_2$-KCl," Appl. Catal., B **254**, 659–666 (2019).
[100]D. Kang, C. Palmer, D. Mannini *et al.*, "Catalytic methane pyrolysis in molten alkali chloride salts containing iron," ACS Catal. **10**, 7032–7042 (2020).
[101]J. Boo, E. H. Ko, N. K. Park *et al.*, "Methane pyrolysis in molten potassium chloride: An experimental and economic analysis," Energies **14**, 8182 (2021).
[102]B. Parkinson, C. F. Patzschke, D. Nikolis *et al.*, "Methane pyrolysis in monovalent alkali halide salts: Kinetics and pyrolytic carbon properties," Int. J. Hydrogen Energy **46**, 6225–6238 (2021).
[103]Y.-G. Noh, Y. J. Lee, J. Kim *et al.*, "Enhanced efficiency in CO_2-free hydrogen production from methane in a molten liquid alloy bubble column reactor with zirconia beads," Chem. Eng. J. **428**, 131095 (2022).
[104]B. Parkinson, C. F. Patzschke, D. Nikolis *et al.*, "Molten salt bubble columns for low-carbon hydrogen from CH_4 pyrolysis: Mass transfer and carbon formation mechanisms," Chem. Eng. J. **417**, 127407 (2021).
[105]C. F. Patzschke, B. Parkinson, J. J. Willis *et al.*, "Co-Mn catalysts for H_2 production via methane pyrolysis in molten salts," Chem. Eng. J. **414**, 128730 (2021).
[106]M. Msheik, S. Rodat, and S. Abanades, "Experimental comparison of solar methane pyrolysis in gas-phase and molten-tin bubbling tubular reactors," Energy **260**, 124943 (2022).
[107]B. Parkinson, J. W. Matthews, T. B. McConnaughy *et al.*, "Techno-economic analysis of methane pyrolysis in molten metals: Decarbonizing natural gas," Chem. Eng. Technol. **40**, 1022–1030 (2017).
[108]T. Ruuska, J. Vinha, and H. Kivioja, "Measuring thermal conductivity and specific heat capacity values of inhomogeneous materials with a heat flow meter apparatus," J. Build. Eng. **9**, 135–141 (2017).
[109]Y. He, H. Chang, D. Wang *et al.*, "Progress of hydrogen production from methane cracking and carbon materials by molten metal method," Chem. Ind. Eng. Prog. **42**, 1270–1280 (2023) (in Chinese).
[110]C.-J. Chen, M. H. Back, and R. A. Back, "The thermal decomposition of methane. I. Kinetics of the primary decompositionto $C_2H6 + H_2$; Rate constant for the homogeneous unimolecular dissociation of methane and its pressure dependence," Can. J. Chem. **53**, 3580–3590 (1975).
[111]C.-J. Chen, M. H. Back, and R. A. Back, "The thermal decomposition of methane. II. Secondary reactions, autocatalysis and carbon formation; Non-Arrhenius behavior in the reaction of CH_3 with ethane," Can. J. Chem. **54**, 3175–3184 (1976).
[112]C. Palmer, M. Tarazkar, M. J. Gordon *et al.*, "Methane pyrolysis in low-cost alkali-halide molten salts at high temperatures," Sustainable Energy Fuels **5**(23), 6107–6123 (2021).
[113]D. Bae, Y. Kim, E. H. Ko *et al.*, "Methane pyrolysis and carbon formation mechanisms in molten manganese chloride mixtures," Appl. Energy **336**, 120810 (2023).
[114]R. A. Dagle, V. Dagle, M. D. Bearden *et al.*, *An Overview of Natural Gas Conversion Technologies for Co-Production of Hydrogen and Value-Added Solid Carbon Products* (Pacific Northwest National Lab, Richland, WA, 2017).